

Summer 2009

Magnetic Stabilization of Nadir-Pointing Small Satellites

Chau Ton

Embry-Riddle Aeronautical University - Daytona Beach

Follow this and additional works at: <https://commons.erau.edu/db-theses>



Part of the [Aerospace Engineering Commons](#), and the [Operations Research, Systems Engineering and Industrial Engineering Commons](#)

Scholarly Commons Citation

Ton, Chau, "Magnetic Stabilization of Nadir-Pointing Small Satellites" (2009). *Theses - Daytona Beach*. 199.

<https://commons.erau.edu/db-theses/199>

This thesis is brought to you for free and open access by Embry-Riddle Aeronautical University – Daytona Beach at ERAU Scholarly Commons. It has been accepted for inclusion in the Theses - Daytona Beach collection by an authorized administrator of ERAU Scholarly Commons. For more information, please contact commons@erau.edu.

Magnetic Stabilization of Nadir-Pointing Small Satellites

By

Chau T. Ton

A thesis submitted to the Physical Sciences Department

In Partial Fulfillment of the Requirements of

Master of Science in Engineering Physics

Embry-Riddle Aeronautical University

Daytona Beach, FL 32114

Summer 2009

UMI Number: EP32002

INFORMATION TO USERS

The quality of this reproduction is dependent upon the quality of the copy submitted. Broken or indistinct print, colored or poor quality illustrations and photographs, print bleed-through, substandard margins, and improper alignment can adversely affect reproduction.

In the unlikely event that the author did not send a complete manuscript and there are missing pages, these will be noted. Also, if unauthorized copyright material had to be removed, a note will indicate the deletion.

UMI[®]

UMI Microform EP32002
Copyright 2011 by ProQuest LLC
All rights reserved. This microform edition is protected against
unauthorized copying under Title 17, United States Code.

ProQuest LLC
789 East Eisenhower Parkway
P.O. Box 1346
Ann Arbor, MI 48106-1346

Copyright by Chau Ton 2009

All Rights Reserved

Magnetic Stabilization of Nadir-Pointing Small Satellites

By Chau Ton

This thesis was prepared under the direction of the candidate's thesis committee chair, Dr. Mahmut Reyhanoglu, Department of Physical Sciences, and has been approved by the members of his thesis committee. It was submitted to the Department of Physical Sciences and was accepted in partial fulfillment of the requirements for the

Degree of

Master of Science in Engineering Physics

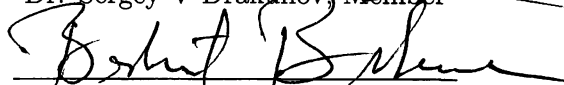
THESIS COMMITTEE:



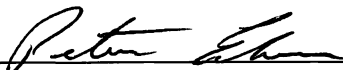
Dr. Mahmut Reyhanoglu, Chair



Dr. Sergey V Drakunov, Member



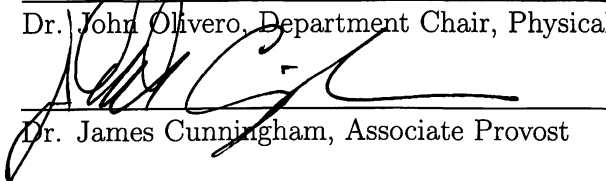
Dr. Bereket Berhane, Member



Dr. Peter Erdman, MSEP Graduate Program Coordinator



Dr. John Olivero, Department Chair, Physical Sciences



Dr. James Cunningham, Associate Provost

6/24/09

Date

Acknowledgments

I would like to thank my advisor, Dr. Mahmut Reyhanoglu, for his guidance and wisdom for the completion of this thesis. I would also want to thank Dr. Drakunov for his guidance toward the subject.

And finally, I would like to thank my parents who have always supported me.

Abstract

Since magnetic control systems are relatively lightweight, require low power and are inexpensive, they are attractive for small, inexpensive satellites in low Earth orbits. In this thesis we present averaging-based feedback control laws that achieve three-axis stabilized nadir-pointing attitude. Two types of nonlinear feedback control laws are proposed: full-state feedback and passivity-based feedback. Full-state feedback uses the attitude and angular velocity measurements to regulate the spacecrafts dynamics. Passivity-based feedback uses the attitude measurement and doesn't require the rate sensors. The control laws are tested using two magnetic field models: the tilted dipole model and the International Geomagnetic Reference Field (IGRF) model. Computer simulations are included to illustrate the effectiveness of the proposed control laws.

Contents

Acknowledgments	iv
Abstract	v
Table of Contents	vi
List of Figures	ix
List of Tables	xi
1 Introduction	2
2 Math Background	4
2.1 Coordinate Systems	4
2.1.1 North East Down Frame	4
2.1.2 Earth Centered Inertial Frame	4
2.1.3 Earth Centered Earth Fixed Frame	5
2.1.4 Perifocal Frame	5
2.1.5 Orbit Frame	5
2.1.6 Body Frame	5
2.2 Coordinate Transformation	6
2.2.1 Introduction to Quaternions	6

2.2.2	Inertia Matrix	12
2.2.3	Transformation from Perifocal Frame to ECI Frame	12
2.2.4	Transformation from ECI Frame to ECEF Frame	13
2.2.5	Transformation from Spherical Coordinates to ECI Frame	13
2.2.6	Transformation from Perifocal Frame to Orbit Frame	14
2.2.7	Transformation from Orbit Frame to Body Frame	14
2.3	Background on Stability	14
2.3.1	Stability	14
3	Mathematical Representation of the Earth's Magnetic Field	18
3.1	IGRF Mathematical Representation	18
3.1.1	Legendre Polynomials	19
3.1.2	Recursive Schmidt Quasi-normalization	21
3.2	Mathematical Modeling of the IGRF in Orbit Frame	22
3.2.1	Geomagnetic Equator and Geographic Equator	22
3.2.2	Transformation from Perifocal Frame to Spherical Coordinates	22
3.2.3	Transformation from ECEF Frame to Orbit Frame	23
3.3	Tilted Dipole Model	24
3.3.1	IGRF and Dipole Magnetic Field Comparison	26
3.4	Further Note	29
4	Mathematical Model	30
4.1	Satellite Model	30
5	Feedback Control Laws	35
5.0.1	Full-State Feedback	35
5.0.2	Passivity-Based Feedback	38

6	Simulation Results	39
6.1	Simulation Results Using the IGRF Model	39
6.1.1	Full-State Feedback	39
6.1.2	Passivity-Based Feedback	47
6.2	Simulation Results for the Tilted Dipole Model	54
6.2.1	Full-State Feedback	54
6.2.2	Passivity-Based Feedback	61
7	Conclusions	68
A	Simulink Diagram	75
B	Matlab m-file	90

List of Figures

2.1	Geocentric Inertial Frame (XYZ) and Orbital Frame ($x_o y_o z_o$)	6
2.2	Direction Cosines	7
2.3	Euler Eigen Axis and Eigen Angle	9
2.4	Geometric Interpretation of Euler's Theorem	10
3.1	Tilted Dipole and IGRF Model Comparison for $i_m = 60^\circ$	27
3.2	Tilted Dipole and IGRF Model Comparison for $i_m = 90^\circ$	28
6.1	Quaternions for $i_m = 60^\circ$ (Full-State Feedback).	41
6.2	Angular Rates for $i_m = 60^\circ$ (Full-State Feedback).	42
6.3	Magnetic Dipole Moments for $i_m = 60^\circ$ (Full-State Feedback).	43
6.4	Quaternions for $i_m = 90^\circ$ (Full-State Feedback).	44
6.5	Angular Rates for $i_m = 90^\circ$ (Full-State Feedback).	45
6.6	Magnetic Dipole Moments for $i_m = 90^\circ$ (Full-State Feedback).	46
6.7	Quaternions for $i_m = 60^\circ$ (Passivity-Based Feedback).	48
6.8	Angular Rates for $i_m = 60^\circ$ (Passivity-Based Feedback).	49
6.9	Magnetic Dipole Moments for $i_m = 60^\circ$ (Passivity-Based Feedback).	50
6.10	Quaternions for $i_m = 90^\circ$ (Passivity-Based Feedback).	51
6.11	Angular Rates for $i_m = 90^\circ$ (Passivity-Based Feedback).	52
6.12	Magnetic Dipole Moments for $i_m = 90^\circ$ (Passivity-Based Feedback).	53

6.13	Quaternions for $i_m = 60^\circ$ (Full-State Feedback).	55
6.14	Angular Rates for $i_m = 60^\circ$ (Full-State Feedback).	56
6.15	Magnetic Dipole Moments for $i_m = 60^\circ$ (Full-State Feedback).	57
6.16	Quaternions for $i_m = 90^\circ$ (Full-State Feedback).	58
6.17	Angular Rates for $i_m = 90^\circ$ (Full-State Feedback).	59
6.18	Magnetic Dipole Moments for $i_m = 90^\circ$ (Full-State Feedback).	60
6.19	Quaternions for $i_m = 60^\circ$ (Passivity-Based Feedback).	62
6.20	Angular Rates for $i_m = 60^\circ$ (Passivity-Based Feedback).	63
6.21	Magnetic Dipole Moments for $i_m = 60^\circ$ (Passivity-Based Feedback).	64
6.22	Quaternions for $i_m = 90^\circ$ (Passivity-Based Feedback).	65
6.23	Angular Rates for $i_m = 90^\circ$ (Passivity-Based Feedback).	66
6.24	Magnetic Dipole Moments for $i_m = 90^\circ$ (Passivity-Based Feedback).	67
A.1	Converting the magnetic field vector from Orbit frame to Body frame.	75
A.2	Modeling the Tilted Dipole Magnetic Field from Perifocal frame and ECEF frame.	76
A.3	Converting the IGRF model from ECI frame to Orbit frame.	77
A.4	Comparing the Tilted Dipole Model and the IGRF model in the Orbit frame.	78
A.5	Checking for longitude and latitude appropriate range and orbital radius Before going into magnetic field calculations.	79
A.6	Calculating the IGRF model.	80
A.7	Converting the Tilted Dipole Magnetic Field Model from Perifocal frame to Orbit frame.	81
A.8	Control Law for the Full-State Feedback.	82
A.9	Control Law for the Passivity-Based Feedback.	83

A.10 The Control Filter State	84
A.11 Transformation Matrix from Geocentric frame to ECEF frame.	85
A.12 Matrix Multiplication going from ECEF frame to Orbit frame.	86
A.13 The spacecraft's coordinate described in Perifocal frame	87
A.14 Modeling of ω	88
A.15 Block diagram of the whole system.	89

List of Tables

7.1	Summary of Simulation Results	68
-----	---	----

Chapter 1

Introduction

It is well known that three independent control torques, generated either via gas jets or momentum wheels, can be used to control the attitude of a rigid spacecraft and that arbitrary reorientation maneuvers of such fully-actuated spacecraft can be accomplished using smooth (or even linear) feedback [30]. If only two independent control torques are available, i.e. if the spacecraft is underactuated [25], the attitude regulation problem cannot be solved using continuous (static or dynamic) time-invariant feedback control laws [5]. In this case, time-varying [19] or discontinuous feedback control laws [13, 12] have been proposed to achieve three-axis attitude control. The discontinuous feedback control laws proposed in [13, 12] for an underactuated spacecraft are based on the general theory developed for nonholonomic control systems [4].

In this paper, the three-axis attitude stabilization problem for a nadir-pointing spacecraft using only magnetic torquers as actuators is studied. Magnetic attitude control is of great use to small satellites due to its lightweight and low power requirements. However, attitude control with sole use of magnetic torquers has the significant challenge that the magnetic torques that can be applied to the spacecraft for attitude control purposes are constrained to lie in the plane orthogonal to the

geomagnetic field vector. This is due to the fact that magnetic torque is given by the cross product of the magnetic dipole moment vector (generated by running currents through the magnetic coils) and the geomagnetic field vector. Although the system is only controllable in two axes that are perpendicular to the local geomagnetic field vector at any point in time, three-axis magnetic stabilization is still possible as the time-variability of the magnetic field along the considered orbit is sufficient to guarantee the stabilizability of the spacecraft. It must be noted that since magnetic torques can be generated only about two axes, the control action required to stabilize the attitude of such spacecraft is inherently nonlinear.

In the literature, several magnetic attitude control schemes have been proposed for satellites in combination with other active or passive attitude stabilization techniques. In particular, magnetic control laws have been developed for spin-stabilized satellites [24, 26, 27, 32], dual-spin satellites [1], gravity-gradient stabilized satellites [2, 35], and momentum-biased satellites [9].

In [17], the problem of inertial attitude regulation for a small spacecraft using only magnetic coils as actuators has been analyzed using averaging technique and it has been shown that a nonlinear low-gain PD-like control law yields (almost) global asymptotic attitude regulation even in the absence of additional active or passive attitude control actuators such as momentum wheels or gravity gradient booms. Other attitude control techniques using solely magnetic actuation can be found in [18, 20, 22, 23, 29, 34]. These techniques include time-varying linear quadratic regulator (LQR) technique [18, 20, 22, 23, 34] and sliding mode control technique [29]. In this thesis, we present averaging-based feedback control laws that achieve three-axis stabilized nadir-pointing attitude for a small satellite.

Chapter 2

Math Background

2.1 Coordinate Systems

This section introduces the different coordinate systems that will be used throughout the thesis.

2.1.1 North East Down Frame

In the North-East-Down (NED) frame, x_n points north, y_n points east, and z_n points towards the center of the earth. The NED frame has its origin fixed on the plane tangent to the Earth's surface. This frame is often used to describe the Earth's magnetic field.

2.1.2 Earth Centered Inertial Frame

The Earth-Centered Inertial (ECI) frame, denoted as I , has its origin at the center of the earth. The Z-axis points toward the north pole, the X-axis points towards the *vernal equinox*. The Y-axis completes the right hand orthogonal system.

2.1.3 Earth Centered Earth Fixed Frame

The Earth Centered Earth Fixed (ECEF) frame, denoted as E , has the same origin as ECI frame, but it rotates along with the earth with a constant angular velocity of $w_e = 7.2921 \cdot 10^{-5} \text{ rad/sec}$.

2.1.4 Perifocal Frame

The Perifocal frame is also known as Earth-Centered Orbital frame. This frame is the natural frame for orbiting satellites. Its x_P -axis points from the focus to the periapse, the z_P -axis is normal to the orbiting plane, and the y_P -axis completes the right hand orthogonal system. This frame will be denoted as P .

2.1.5 Orbit Frame

The Orbit frame, denoted as O , has its origin at the center of mass of the spacecraft. The x_o -axis is in direction of the velocity, the z_o -axis points toward the center of the earth, and the y_o completes the right hand orthogonal system.

2.1.6 Body Frame

The Body Frame, denoted as B , has its origin at the center of mass of the spacecraft. Unlike the Orbit frame, it has its origin fixed at the center of mass of the spacecraft.

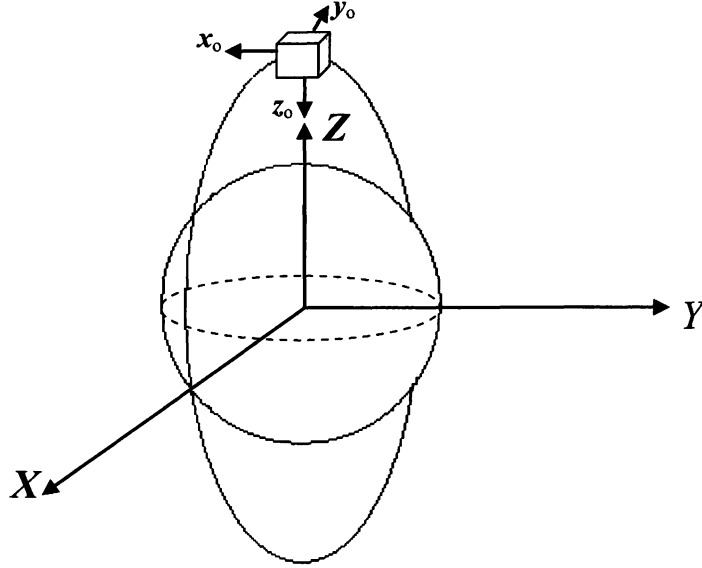


Figure 2.1: Geocentric Inertial Frame (XYZ) and Orbital Frame ($x_0y_0z_0$)

2.2 Coordinate Transformation

In order to effectively model spacecraft attitude, it's necessary to convert the results into workable coordinates. This section will describe the transformation matrix that's being used to switch between coordinate frames.

2.2.1 Introduction to Quaternions

The most commonly used sets of attitude parameters are the Euler angles. They describe the attitude of one frame relative to another. The Euler angles provide a compact, three-parameter attitude description whose coordinates are easy to visualize. One major drawback of these angles is that they result in a geometric singularity. Therefore, their use in describing large rotations is limited. Also, both the rotation matrix and the kinematic equations are highly nonlinear and involve numerous computations of trigonometric functions. Quaternions provide a four-parameter

singularity free representation that does not require the calculation of any trigonometric functions. Quaternions, unlike Euler angles, use one axis called an eigenaxis to rotate between coordinate systems. In this chapter, we first briefly review the attitude kinematics and dynamics formulation used in this thesis to obtain the rotational equations of motion for a group of spacecraft. For full details, the reader is referred to [33].

Reference Frames and Rotations

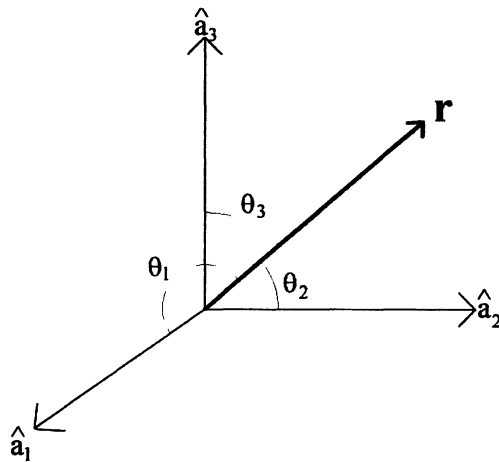


Figure 2.2: Direction Cosines

Consider a right-handed orthonormal reference frame A , whose three unit vectors are \hat{a}_1 , \hat{a}_2 , and \hat{a}_3 . Let $\cos \theta_1$, $\cos \theta_2$, and $\cos \theta_3$ be the direction cosines of a vector \mathbf{r} as shown in Figure 2.2. Then, we write

$$\mathbf{r} = r (\hat{a}_1 \cos \theta_1 + \hat{a}_2 \cos \theta_2 + \hat{a}_3 \cos \theta_3) ,$$

where r is the length of \mathbf{r} . Now consider another right-handed orthonormal reference frame B with three unit vectors \hat{b}_1 , \hat{b}_2 , and \hat{b}_3 . A relation between the two reference frames A and B can be written as:

$$\begin{bmatrix} \hat{b}_1 \\ \hat{b}_2 \\ \hat{b}_3 \end{bmatrix} = \begin{bmatrix} r_{11} & r_{12} & r_{13} \\ r_{21} & r_{22} & r_{23} \\ r_{31} & r_{32} & r_{33} \end{bmatrix} \begin{bmatrix} \hat{a}_1 \\ \hat{a}_2 \\ \hat{a}_3 \end{bmatrix},$$

where r_{ij} is the direction cosine between \hat{b}_i and \hat{a}_j . The matrix

$$\mathbf{R} = \begin{bmatrix} r_{11} & r_{12} & r_{13} \\ r_{21} & r_{22} & r_{23} \\ r_{31} & r_{32} & r_{33} \end{bmatrix},$$

is an orthonormal rotation matrix with the following properties:

$$\mathbf{R}\mathbf{R}^T = \mathbf{R}^T\mathbf{R} = \mathbf{I}, \det(\mathbf{R}) = +1,$$

where \mathbf{I} is the 3x3 identity matrix. Let \mathbf{r}_A represent a vector in terms of its components in the frame A . Then, the vector can be represented in the frame B as

$$\mathbf{r}_B = \mathbf{R}\mathbf{r}_A, \tag{2.1}$$

where \mathbf{R} is the rotation matrix from frame A to B .

Eulers theorem states that the general rotation of a rigid body with one fixed point is a rotation about an axis through that point. Figure 2.3 illustrates the geometry pertaining to Eulers theorem. Now consider an arbitrary vector \mathbf{r} as shown in Figure 2.4. As frame A rotates about an axis \mathbf{e} (called an eigenaxis), by an angle θ (called

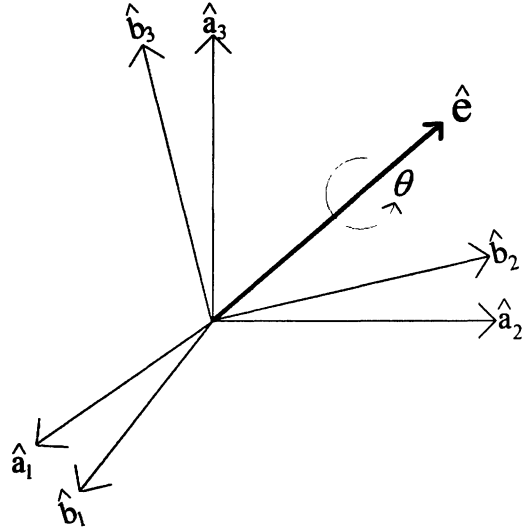


Figure 2.3: Euler Eigen Axis and Eigen Angle

an eigenangle), it will appear to an observer fixed in A that \mathbf{r} is rotating about \mathbf{e} through an angle $-\theta$; to this observer, the rotation corresponds to $\mathbf{r} \rightarrow \mathbf{r}'$, where

$$\mathbf{r}' = (\mathbf{e} \cdot \mathbf{r}) \mathbf{e} - \mathbf{e} \times (\mathbf{e} \times \mathbf{r}) \cos \theta - \mathbf{e} \times \mathbf{r} \sin \theta .$$

Note that $\mathbf{e}^T \mathbf{e} = 1$. The components of \mathbf{r}' in B can then be written as

$$\mathbf{r}_B = [\mathbf{e}\mathbf{e}^T + (\mathbf{I} - \mathbf{e}\mathbf{e}^T) \cos \theta - \tilde{\mathbf{e}} \sin \theta] \mathbf{r}_A ,$$

where $\tilde{\mathbf{e}}$ denotes the skew symmetric matrix satisfying $\mathbf{e} \times \mathbf{r} = \tilde{\mathbf{e}}\mathbf{r}$, and is given by

$$\tilde{\mathbf{e}} = \begin{bmatrix} 0 & -e_3 & e_2 \\ e_3 & 0 & -e_1 \\ -e_2 & e_1 & 0 \end{bmatrix} \quad (2.2)$$

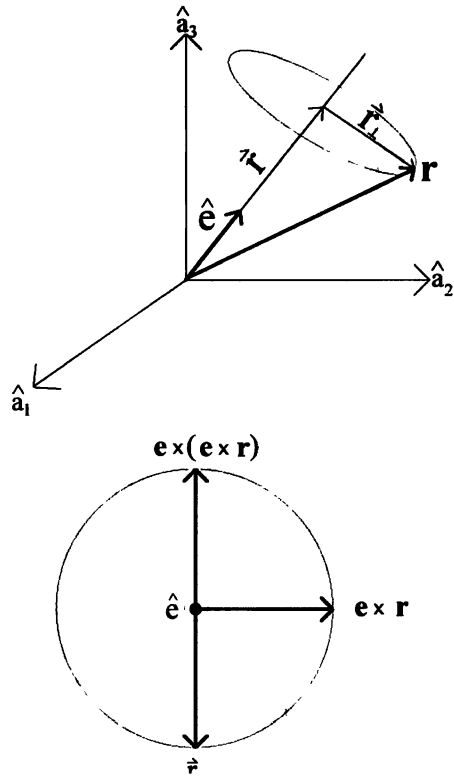


Figure 2.4: Geometric Interpretation of Euler's Theorem

In full matrix form, the rotation matrix becomes

$$\mathbf{R} = \begin{bmatrix} c\theta + e_1^2(1 - c\theta) & e_1e_2(1 - c\theta) + e_3s\theta & e_1e_3(1 - c\theta) - e_2s\theta \\ e_2e_1(1 - c\theta) - e_3s\theta & c\theta + e_2^2(1 - c\theta) & e_2e_3(1 - c\theta) + e_1s\theta \\ e_3e_2(1 - c\theta) + e_2s\theta & e_3e_2(1 - c\theta) - e_1s\theta & c\theta + e_3^2(1 - c\theta) \end{bmatrix},$$

where $c\theta \triangleq \cos \theta$ and $s\theta \triangleq \sin \theta$.

Unit Quaternions

The unit quaternions are defined as

$$\mathbf{q} = \begin{bmatrix} \mathbf{q}_v \\ q_4 \end{bmatrix} = \begin{bmatrix} e_1 \sin \frac{\theta}{2} \\ e_2 \sin \frac{\theta}{2} \\ e_3 \sin \frac{\theta}{2} \\ \cos \frac{\theta}{2} \end{bmatrix} = \begin{bmatrix} q_1 \\ q_2 \\ q_3 \\ q_4 \end{bmatrix}. \quad (2.3)$$

The quaternions are constrained by

$$\mathbf{q}^T \mathbf{q} = q_1^2 + q_2^2 + q_3^2 + q_4^2 = 1, \quad (2.4)$$

where \mathbf{q}_v is the vector part of the quaternions, and q_4 is the scalar part.

The rotation matrix can be parameterized in terms of quaternions as

$$\mathbf{R} = \begin{bmatrix} 1 - 2(q_2^2 + q_3^2) & 2(q_1q_2 + q_3q_4) & 2(q_1q_3 - q_2q_4) \\ 2(q_1q_2 - q_3q_4) & 1 - 2(q_1^2 + q_3^2) & 2(q_2q_3 + q_1q_4) \\ 2(q_1q_3 + q_2q_4) & 2(q_2q_3 - q_1q_4) & 1 - 2(q_1^2 + q_2^2) \end{bmatrix}. \quad (2.5)$$

The unit quaternion \mathbf{q} can be thought as a hypercomplex quantity that has three imaginary parts \mathbf{q}_v and one real part q_4 .

Quaternion Multiplication

Multiplication of two quaternions is denoted by $\mathbf{q}_1 \mathbf{q}_2 = \mathbf{Q}(\mathbf{q}_1) \mathbf{q}_2$, where

$$\mathbf{Q}(\mathbf{q}) = \begin{pmatrix} q_4 \mathbf{I} + \tilde{\mathbf{q}}_v & \mathbf{q}_v \\ -\mathbf{q}_v^T & q_4 \end{pmatrix}, \quad (2.6)$$

and \mathbf{I} is a 3×3 identity matrix.

Quaternion Error

The quaternion error can be expressed in terms of the actual attitude \mathbf{q} and the desired attitude \mathbf{q}_d as

$$\mathbf{q}_e = \mathbf{q}^* \mathbf{q}_d = \begin{pmatrix} \mathbf{q}_{ve} \\ q_{4e} \end{pmatrix}, \quad (2.7)$$

where \mathbf{q}^* is the inverse quaternion of \mathbf{q}

$$\mathbf{q}^* = \begin{pmatrix} \mathbf{q}_v \\ q_4 \end{pmatrix}^* = \begin{pmatrix} -\mathbf{q}_v \\ q_4 \end{pmatrix}. \quad (2.8)$$

2.2.2 Inertia Matrix

The spacecraft's inertia matrix is given by

$$\mathbf{J} = \begin{bmatrix} J_1 & 0 & 0 \\ 0 & J_2 & 0 \\ 0 & 0 & J_3 \end{bmatrix}. \quad (2.9)$$

To simplify the presentation of the main ideas, an iso-inertial spacecraft is considered, so $J_1 = J_2 = J_3 = J$. This simplification will allow the elimination of gravity gradient terms in the control torque.

2.2.3 Transformation from Perifocal Frame to ECI Frame

The transformation matrix to go from Perifocal to ECI frame requires three elements: the right ascension Ω , argument of perigee ω , and inclination angle i . The matrix is

given as follow

$$\mathbf{R}_P^I = \begin{bmatrix} \cos \Omega \cos \omega - \sin \Omega \sin \omega \cos i & -\cos \Omega \sin \omega - \sin \Omega \cos i \cos \omega & \sin \Omega \sin i \\ \sin \Omega \cos \omega + \cos \Omega \cos i \sin \omega & -\sin \Omega \sin \omega + \cos \Omega \cos i \cos \omega & -\cos \Omega \sin i \\ \sin i \sin \omega & \sin i \cos \omega & \cos i \end{bmatrix}. \quad (2.10)$$

2.2.4 Transformation from ECI Frame to ECEF Frame

Transforming from ECI to ECEF frame is given as

$$\mathbf{R}_I^E = \begin{bmatrix} \cos w_e t & \sin w_e t & 0 \\ -\sin w_e t & \cos w_e t & 0 \\ 0 & 0 & 1 \end{bmatrix}, \quad (2.11)$$

where $w_e = 7.2921 \cdot 10^{-5} \text{ rad/sec}$ is the angular velocity of the Earth.

2.2.5 Transformation from Spherical Coordinates to ECI Frame

The spherical coordinate is in the same frame as the ECEF frame. Transforming from spherical to ECI frame is given as

$$\mathbf{R}_S^I = \begin{bmatrix} \cos \delta \cos \alpha & \sin \delta \cos \alpha & -\sin \alpha \\ \cos \delta \sin \alpha & \sin \delta \sin \alpha & \cos \alpha \\ \sin \delta & -\cos \delta & 0 \end{bmatrix}, \quad (2.12)$$

where $\delta = 90^\circ - \theta$, and $\alpha = \phi + w_e t$. Note that θ is the co-latitude and ϕ is the longitude.

2.2.6 Transformation from Perifocal Frame to Orbit Frame

Transforming from Perifocal to Orbit frame is given as

$$\mathbf{R}_P^O = \begin{bmatrix} -\sin nt & \cos nt & 0 \\ 0 & 0 & -1 \\ -\cos nt & -\sin nt & 0 \end{bmatrix}. \quad (2.13)$$

2.2.7 Transformation from Orbit Frame to Body Frame

The transformation matrix from Orbit frame to Body frame is given by Wie as

$$\mathbf{R}_O^B = (q_4^2 - \mathbf{q}_v^T \mathbf{q}_v) \mathbf{I} + 2\mathbf{q}_v \mathbf{q}_v^T - 2q_4 \tilde{\mathbf{q}}_v, \quad (2.14)$$

where $\mathbf{q}_v = [q_1 \ q_2 \ q_3]^T$, and $\tilde{\mathbf{q}}_v$ is the skew symmetric matrix

$$\tilde{\mathbf{q}}_v = \begin{bmatrix} 0 & -q_3 & q_2 \\ q_3 & 0 & -q_1 \\ -q_2 & q_1 & 0 \end{bmatrix}.$$

2.3 Background on Stability

This section explains the Theorems Principle of this thesis. Discussions of stability, especially Lyapunov stability will be covered. Most of the materials found in this section can be found in [33].

2.3.1 Stability

Let's define

$$\dot{\mathbf{x}} = \mathbf{f}(\mathbf{x}, t), \quad (2.15)$$

where $\mathbf{f}(\mathbf{x}, t)$ is a nonlinear function for all x and t , and $\mathbf{x} = (x_1, \dots, x_n)$. Let x^* be the equilibrium state satisfying

$$\mathbf{f}(\mathbf{x}^*, t) = 0 . \quad (2.16)$$

Positive Definite Functions

A function $V(x)$ is defined as definite positive if $V(0) = 0$ and $V(x) > 0$ for $x \neq x^*$.

It is semi-definite positive if $V(0) = 0$ and $V(x) \geq 0$ for $x \neq x^*$.

A function $V(x)$ is definite negative if $V(0) = 0$ and $V(x) < 0$ for $x \neq x^*$. It is semi-definite negative if $V(0) = 0$ and $V(x) \leq 0$ for $x \neq x^*$.

Lyapunov Stability

The equilibrium state x^* is said to be Lyapunov stable if for any $\epsilon > 0$ there exists a real and positive number $\delta(\epsilon, t_0)$ such that

$$\|\mathbf{x}(t_0) - \mathbf{x}^*\| \leq \delta(\epsilon, t_0) \Rightarrow \|\mathbf{x}(t) - \mathbf{x}^*\| \leq \epsilon \quad \text{for all } t \geq t_0 , \quad (2.17)$$

where $\|\mathbf{x}\| = \sqrt{\mathbf{x}^T \mathbf{x}}$.

Local Asymptotic Stability

A system is said to be locally asymptotically stable if an isolated equilibrium point \mathbf{x}^* is Lyapunov stable and if there exists a positive $\bar{\delta}$ such that

$$\|\mathbf{x}(t_0) - \mathbf{x}^*\| \leq \bar{\delta} \Rightarrow \mathbf{x}(t) \rightarrow \mathbf{x}^* \quad \text{as } t \rightarrow \infty . \quad (2.18)$$

Global Asymptotic Stability

A system is said to be globally asymptotically stable if an isolated equilibrium point \mathbf{x}^* is Lyapunov stable and

$$\mathbf{x}(t) \rightarrow \mathbf{x}^* \quad \text{as } t \rightarrow \infty, \quad (2.19)$$

for any initial condition $\mathbf{x}(t_0)$.

Lyapunov's Direct Stability Theorem

If there exists in some finite neighborhood D of the equilibrium point \mathbf{x}^* a positive-definite scalar function $E(x)$ with continuous first partial derivatives with respect to \mathbf{x} that satisfies the following conditions:

1. If $E(\mathbf{x}) > 0$ and $\dot{E}(\mathbf{x}) \leq 0$ for $\mathbf{x} \neq \mathbf{x}^*$, and $E(\mathbf{x}^*) = 0$ for all t , then the equilibrium point at \mathbf{x}^* is Lyapunov stable.
2. In addition to the condition above, if $\dot{E}(\mathbf{x})$ is not identically zero along any solution \mathbf{x} other than \mathbf{x}^* , then the system is locally asymptotically stable.
3. If, in addition, there exists in the entire state space a positive-definite function $E(\mathbf{x})$ which is radially unbounded, then the equilibrium point \mathbf{x}^* is globally asymptotically stable.

Averaging Method

Averaging is a method of approximating the dynamics of a (slowly) time-varying system by the dynamics of a time-invariant averaged system (see e.g. [11]). More precisely, let

$$\dot{\mathbf{x}} = \epsilon \mathbf{f}(\mathbf{x}, t, \epsilon).$$

Here $\epsilon > 0$ is a small parameter which models the fact that the dynamics of \mathbf{x} are slowly varying with respect to the variation of the right hand side of the above equation. The averaged system is described by

$$\dot{\mathbf{x}}_{av} = \epsilon \mathbf{f}((x)_{av}) ,$$

where

$$\mathbf{f}((x)_{av}) = \lim_{T \rightarrow \infty} \frac{1}{T} \int_{t_0}^{t_0+T} \mathbf{f}(\mathbf{x}, \tau, 0) d\tau ,$$

assuming that limit existis.

According to the generalized averaging theory [11], if the averaged system is exponentially stable, there exists an $\epsilon^* > 0$ such that for $0 < \epsilon < \epsilon^*$ the original nonlinear system is exponentially stable.

Chapter 3

Mathematical Representation of the Earth's Magnetic Field

3.1 IGRF Mathematical Representation

As presented in [11] the magnetic field is expressed as the negative gradient of the scalar potential

$$\mathbf{B} = -\nabla V . \quad (3.1)$$

The IGRF uses spherical harmonic to model the scalar potential as

$$V(r, \theta, \phi) = a \sum_{n=1}^k \left(\frac{a}{r}\right)^{n+1} \sum_{m=0}^n (g_n^m \cos m\phi + h_n^m \sin m\phi) P_n^m(\theta) . \quad (3.2)$$

The coordinate system that the IGRF uses is geocentric coordinate, r is the radius from the center of the earth to orbit, θ is the co-latitude with respect to the geographic equator, and ϕ is the longitude. The symbol a stands for the Earth's radius, which is 6371.2 km . The coefficient g_n^m and h_n^m are Gaussian coefficients, and $P_n^m(\cos \theta)$ is the Schmidt quasi-normalized associated Legendre functions of order m and degree n .

Breaking the magnetic field components from equation (3.2) as in [11] , we obtain

$$B_r = \sum_{n=1}^k \left(\frac{a}{r}\right)^{n+2} (n+1) \sum_{m=0}^n (g^{n,m} \cos m\phi + h^{n,m} \sin m\phi) P^{n,m}(\theta) , \quad (3.3)$$

$$B_\theta = -\sum_{n=1}^k \left(\frac{a}{r}\right)^{n+2} \sum_{m=0}^n (g^{n,m} \cos m\phi + h^{n,m} \sin m\phi) \frac{\partial P^{n,m}(\theta)}{\partial \theta} , \quad (3.4)$$

$$B_\phi = \frac{-1}{\sin \theta} \sum_{n=1}^k \left(\frac{a}{r}\right)^{n+2} \sum_{m=0}^n m (-g^{n,m} \sin m\phi + h^{n,m} \cos m\phi) P^{n,m}(\theta) , \quad (3.5)$$

where B_r , B_θ , and B_ϕ are the magnetic field components in its spherical coordinate.

Also $P^{n,m}(\theta)$ is the Gaussian normalized associated Legendre polynomials.

3.1.1 Legendre Polynomials

In order to get to Schmidt quasi-normalized Legendre functions, we must start with the Legendre polynomials $P_n(t)$, which is

$$(1 - 2tx + x^2)^{-1/2} = \sum_{n=0}^{\infty} P_n(t) x^n . \quad (3.6)$$

When solving for $P_n(t)$, one ends up with Rodrigues's formula

$$P_n(t) = \frac{1}{2^n n!} \left(\frac{d}{dt}\right)^n (t^2 - 1)^n . \quad (3.7)$$

Associated Legendre Polynomials

The associated Legendre Polynomials has the following relationship with Rodrigues's formula

$$P_{n,m}(t) = (1 - t^2)^{1/2m} \frac{d^m}{dt^m} (P_n(t)) . \quad (3.8)$$

The associated Legendre polynomials equals to zero when m is greater than n .

Gaussian Normalized Associated Legendre Polynomials

The Gaussian normalized Associated Legendre polynomials relate to $P_{n,m}$ as

$$P^{n,m} = \frac{2^n!(n-m)!}{(2n)!} P_{n,m} . \quad (3.9)$$

Equation (3.9) is one of the normalizations of Legendre polynomials. The normalization that we are interested in is the Schmidt quasi-normalization.

Schmidt Quasi-normalized Associated Legendre Functions

Schmidt quasi-normalized associated Legendre functions in relation to the associated Legendre polynomials is

$$P_n^m = \left[\frac{2(n-m)!}{(n+m)!} \right]^{1/2} P_{n,m} . \quad (3.10)$$

The relationship between the Schmidt quasi-normalization and Gaussian normalization is

$$P_n^m = S_{n,m} P^{n,m} , \quad (3.11)$$

where $S_{n,m}$ is

$$S_{n,m} = \left[\frac{(2 - \delta_m^0)(n-m)!}{(n+m)!} \right]^{1/2} \frac{(2n-1)!!}{(n-m)!} , \quad (3.12)$$

where $(2n-1)!! = 1 \cdot 3 \cdot 5 \cdots (2n-1)$. The Kronecker delta function is $\delta_i^j = 1$ if $i = j$ and $\delta_i^j = 0$ if $i \neq j$.

The relationship of the coefficient g_n^m and h_n^m from the Gaussian normalization

and $g^{n,m}$ and $h^{n,m}$ can be described by

$$g^{n,m} = S_{n,m} g_n^m, \quad (3.13)$$

$$h^{n,m} = S_{n,m} h_n^m. \quad (3.14)$$

The coefficients g_n^m and h_n^m are provided by the IGRF every five years.

3.1.2 Recursive Schmidt Quasi-normalization

In order to optimize the code to run faster, it's easy to see that the recursive form of the Schmidt normalization factor can be used as

$$S_{0,0} = 1 \quad n = m, \quad (3.15)$$

$$S_{n,0} = S_{n-1,0} \left[\frac{2n-1}{n} \right] \quad n \geq 1, \quad (3.16)$$

$$S_{n,m} = S_{n,m-1} \sqrt{\frac{(n-m+1)(\delta_m^1+1)}{n+m}} \quad m \geq 1. \quad (3.17)$$

The Gaussian normalized Legendre polynomial can be described in a recursive relationship as follows

$$P^{0,0} = 1, \quad (3.18)$$

$$P^{n,n} = \sin \theta P^{n-1,n-1}, \quad (3.19)$$

$$P^{n,m} = \cos \theta P^{n-1,m} - K^{n,m} P^{n-2,m}, \quad (3.20)$$

where

$$K^{n,m} = 0 \quad n = 1, \quad (3.21)$$

$$K^{n,m} = \frac{(n-1)^2 - m^2}{(2n-1)(2n-3)} \quad n > 1. \quad (3.22)$$

The partial derivative of the Legendre polynomials has the following recursive formula

$$\frac{\partial P^{0,0}}{\partial \theta} = 0, \quad (3.23)$$

$$\frac{\partial P^{n,n}}{\partial \theta} = \sin \theta \frac{\partial P^{n-1,n-1}}{\partial \theta} + \cos \theta P^{n-1,n-1}, \quad (3.24)$$

$$\frac{\partial P^{n,m}}{\partial \theta} = \cos \theta \frac{\partial P^{n-1,m}}{\partial \theta} - K^{n,m} \frac{\partial P^{n-2,m}}{\partial \theta}. \quad (3.25)$$

3.2 Mathematical Modeling of the IGRF in Orbit Frame

3.2.1 Geomagnetic Equator and Geographic Equator

Geomagnetic equator is the equator based on the magnetic field of the earth. The best fit line of the magnetic equator of the dipole with respect to the geographic equator is offset approximately by 11.5° in the 2005 [18]. If we model the polar orbit, where $i_m = 90^\circ$, then the inclination with respect geographic equator is $i = i_m + 11.5^\circ$. In this case, the orbit would be retrograde.

3.2.2 Transformation from Perifocal Frame to Spherical Coordinates

The satellite's position in the Perifocal frame is described as

$$\mathbf{r}_P = r \begin{bmatrix} \cos nt \\ \sin nt \\ 0 \end{bmatrix}, \quad (3.26)$$

where r is the orbit radius.

To transform the satellite's position from Perifocal to ECEF frame, which can be transformed into spherical coordinates, the following transformation matrixes are applied as

$$\mathbf{R}_P^E = \mathbf{R}_I^E \mathbf{R}_P^I . \quad (3.27)$$

Now the satellite's position in the Perifocal frame with respect the ECEF frame is described as

$$\begin{bmatrix} X_E \\ Y_E \\ Z_E \end{bmatrix} = \mathbf{R}_P^E \begin{bmatrix} X_P \\ Y_P \\ Z_P \end{bmatrix} . \quad (3.28)$$

From this, it can be simply transformed into spherical coordinate as follows

$$r = \sqrt{X_E^2 + Y_E^2 + Z_E^2} , \quad (3.29)$$

$$\phi = \tan^{-1} \frac{Y_E}{X_E} , \quad (3.30)$$

$$\theta = \cos^{-1} \frac{Z_E}{r} . \quad (3.31)$$

From r , ϕ , and θ obtained above, the magnetic field of the earth can be obtained using (3.3)-(3.5).

3.2.3 Transformation from ECEF Frame to Orbit Frame

Once the magnetic field of the earth is calculated, the transformation from spherical coordinate frame to Orbit frame can be done as follows

$$\mathbf{B}_O = \mathbf{R}_P^O \mathbf{R}_I^P \mathbf{R}_S^I \mathbf{B}_{r,\theta,\phi} . \quad (3.32)$$

Note that $\mathbf{R}_P^I = (\mathbf{R}_I^P)^T$.

3.3 Tilted Dipole Model

This section covers the tilted dipole model that has its origin at the center of the earth [18]. The tilted dipole model comes from the first three terms of the spherical harmonic model:

$$V(r, \theta, \phi) = \frac{a^3}{r^2} [g_1^0 P_1^0(\theta) + (g_1^1 \cos \phi + h_1^1 \sin \phi) P_1^1(\theta)] , \quad (3.33)$$

$$= \frac{a^3}{r^2} [g_1^0 \cos \theta + g_1^1 \cos \phi \sin \theta + h_1^1 \sin \phi \sin \theta] . \quad (3.34)$$

The co-elevation θ_m and the East longitude ϕ_m of the tilted dipole are given by

$$\theta_m = \cos^{-1} \left(\frac{g_1^0}{H_o} \right) , \quad (3.35)$$

$$\phi_m = \tan^{-1} \left(\frac{h_1^1}{g_1^1} \right) . \quad (3.36)$$

The constant H_o is the magnitude based on the first three term, i.e.

$$H_o = \sqrt{(g_1^0)^2 + (g_1^1)^2 + (h_1^1)^2} . \quad (3.37)$$

Solving for the first three terms of the IGRF model, one ends up with

$$B_r = 2 \left(\frac{R_e}{r} \right)^3 [g_1^0 \cos \theta + (g_1^1 \cos \phi + h_1^1 \sin \phi) \sin \theta] , \quad (3.38)$$

$$B_\theta = \left(\frac{R_e}{r} \right)^3 [g_1^0 \sin \theta - (g_1^1 \cos \phi + h_1^1 \sin \phi) \cos \theta] , \quad (3.39)$$

$$B_\phi = \left(\frac{R_e}{r} \right)^3 [g_1^0 \sin \phi - h_1^1 \cos \phi] . \quad (3.40)$$

Assuming that the Earth's magnetic field is aligned with the dipole strength and the magnetic north is from the above calculation of θ_m and ϕ_m , the tilted dipole can be represented as

$$\mathbf{B} = \frac{a}{r} H_o [(\hat{\mathbf{r}} \cdot \hat{\mathbf{m}})\hat{\mathbf{r}} - \hat{\mathbf{m}}] , \quad (3.41)$$

where \mathbf{r} is the position vector, $\hat{\mathbf{r}}$ is the unit vector in the direction of \mathbf{r} , and r is the orbital radius

$$\hat{\mathbf{m}} = \begin{bmatrix} \sin \theta_m \cos \alpha_m \\ \sin \theta_m \sin \alpha_m \\ \cos \theta_m \end{bmatrix} , \quad (3.42)$$

where

$$\alpha_m = \theta_{g0} + w_e t + \phi_m . \quad (3.43)$$

Here α_m is defined as the Greenwich sidereal at a reference time. Note that the dipole model result is obtained in the geocentric inertial frame. For the 2005 IGRF model, $g_1^0 = -29556.8nT$, $g_1^1 = -1671.8nT$, and $h_1^1 = 5080.0nT$, so the co-elevation and East longitude are $\theta_m = 169.744^\circ$ and $\phi_m = 288.216^\circ$. The results show that the north magnetic pole is pointing toward the Southern Hemisphere. The north magnetic pole intersect at 79.556°N and 288.216°E .

If we make the approximation that $\theta_m = 180^\circ$, $\omega = 0^\circ$, and $\Omega = 0^\circ$, we can model the dipole magnetic field in the orbit frame as

$$\mathbf{B}_O = \frac{\mu_m}{r^3} \begin{bmatrix} \cos nt \sin i_m \\ -\cos i_m \\ 2 \sin nt \sin i_m \end{bmatrix}, \quad (3.44)$$

where i_m is the inclination of the spacecraft's orbit with respect to the magnetic equatorial equator, and μ_m is the total Earth's dipole strength, which is around $10^{16} \text{ Wb} \cdot \text{m}$. When $t = 0$, the spacecraft starts at the intersection of the ascending node and the magnetic equator. This model assumes that the dipole is none-rotating and it ignores the Earth's oblateness. At low Earth orbits, the magnetic field is significant, therefore magnetic torquers can be used.

3.3.1 IGRF and Dipole Magnetic Field Comparison

Below are plots comparing the IGRF and tilted dipole model in the orbit frame for $i_m = 60^\circ$ and $i_m = 90^\circ$. It can be seen from the graphs that the two models are relatively close to each other; thus, the tilted dipole model can be used in the simulations and still yield good results.

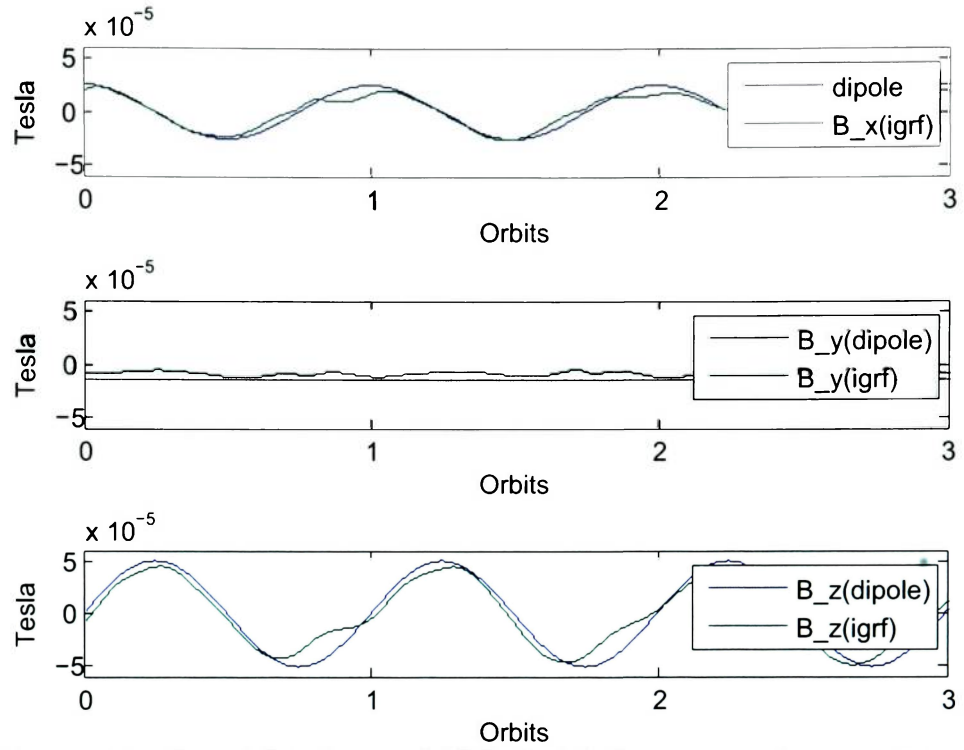


Figure 3.1: Tilted Dipole and IGRF Model Comparison for $i_m = 60^\circ$.

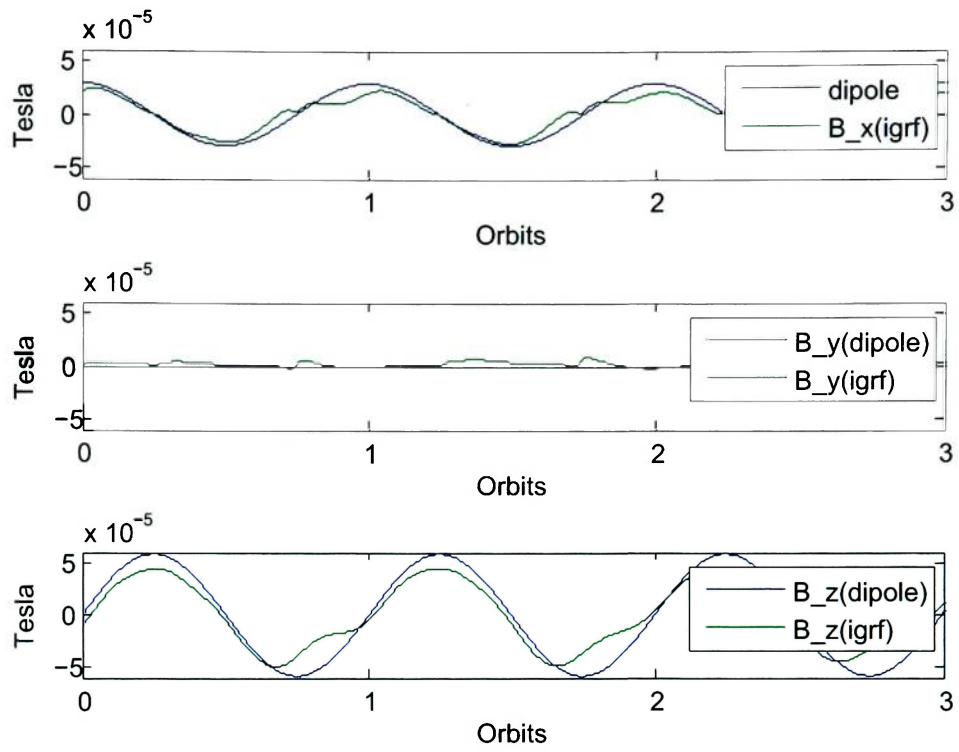


Figure 3.2: Tilted Dipole and IGRF Model Comparison for $i_m = 90^\circ$.

3.4 Further Note

The IGRF model only take into account the averages of the Earth's magnetic field over the course of five years. There are interferences that the IGRF are not accounted for, i.e solar radiation from the sun, substorm, very local magnetization, etc.

Chapter 4

Mathematical Model

4.1 Satellite Model

Let $\boldsymbol{\omega}$ be the angular velocity of the satellite with respect to the geocentric inertial frame I expressed in the body frame B . Then the angular velocity of the body frame relative to the orbit frame can be expressed as [21]

$$\boldsymbol{\omega}_r = \boldsymbol{\omega} - \mathbf{R}\boldsymbol{\omega}_O, \quad (4.1)$$

where $\boldsymbol{\omega}_O$ is the angular velocity, in O , of O relative to the inertial frame.

Let \mathbf{r}_x , \mathbf{r}_y , \mathbf{r}_z denote the columns of the rotation matrix \mathbf{R} . Then, since

$$\boldsymbol{\omega}_O = [0, -n, 0]^T, \quad (4.2)$$

where n is the orbital rate, equation (4.1) can be written as

$$\boldsymbol{\omega}_r = \boldsymbol{\omega} + n\mathbf{r}_y. \quad (4.3)$$

The attitude kinematics can now be written in terms of quaternions as

$$\dot{\mathbf{q}} = \frac{1}{2} \mathbf{Q}_v(\mathbf{q})(\boldsymbol{\omega} + n\mathbf{r}_y), \quad (4.4)$$

where

$$\mathbf{Q}_v(\mathbf{q}) = \begin{pmatrix} q_4 \mathbf{I} + \tilde{\mathbf{q}}_v \\ -\mathbf{q}_v^T \end{pmatrix}.$$

Denote by $\boldsymbol{\tau}$ the control torque vector in the Body frame B . Then, the attitude dynamics can be expressed as

$$\mathbf{J}\dot{\boldsymbol{\omega}} + \boldsymbol{\omega} \times \mathbf{J}\boldsymbol{\omega} = \boldsymbol{\tau} + 3n^2 \mathbf{r}_z \times \mathbf{J} \mathbf{r}_z, \quad (4.5)$$

where $\mathbf{J} = \text{diag}\{J_x, J_y, J_z\}$ is the inertia matrix of the spacecraft and $3n^2 \mathbf{r}_z \times \mathbf{J} \mathbf{r}_z$ is the gravity-gradient torque.

In this thesis, for simplicity in presenting the ideas, we will consider an isoinertial spacecraft (i.e. $J_x = J_y = J_z = J$) so that equation (4.5) reduces to

$$J\dot{\boldsymbol{\omega}} = \boldsymbol{\tau}. \quad (4.6)$$

Magnetic torquers operate in accordance with the magnetic torque equation given by

$$\boldsymbol{\tau} = \mathbf{M} \times \mathbf{B} = \tilde{\mathbf{M}}\mathbf{B}, \quad (4.7)$$

where \mathbf{B} is the geomagnetic field vector and \mathbf{M} is the magnetic dipole moment vector (which represents the actual control vector) generated by running currents through the magnetic coils. The control action is inherently nonlinear and difficult to use since the control torque can only be generated perpendicular to the geomagnetic field vector. As mentioned previously, the system is underactuated since a rigid spacecraft

has three rotational degrees of freedom while magnetic torques can only be generated about two axes. It has been shown in [3] that if the magnetic field is periodic in time, then the attitude dynamics of the spacecraft are controllable. Moreover, the attitude dynamics of a spacecraft actuated by three magnetic actuators in a closed Keplerian orbit in a nonrotating dipole approximation of the geomagnetic field are strongly accessible and controllable if the orbital plane does not coincide with the geomagnetic equatorial plane.

The three axis magnetorquer control system considered in this paper consists of three orthogonal copper coils. Current supplied to the copper wire produces a magnetic dipole which interacts with the magnetic field of the Earth to produce control torques. The magnetic dipole moment vector generated by the coils can be expressed in the body frame B as

$$\mathbf{M} = \begin{bmatrix} M_x \\ M_y \\ M_z \end{bmatrix} = \begin{bmatrix} N_x I_x A_x \\ N_y I_y A_y \\ N_z I_z A_z \end{bmatrix}, \quad (4.8)$$

where, for $k = x, y, z$, N_k is the number of windings of the magnetic coil on the axis in the k -direction, I_k is the current in the coil and A_k is the coil area.

As explained earlier, a commonly used model of the Earth's magnetic field is known as the IGRF model (International Geomagnetic Reference Model). In this thesis, for analytic purposes, we will also model the Earth's magnetic field as a dipole (bar magnet). Assuming a nonrotating dipole and neglecting the regression of the line of nodes due to the Earth's oblateness, the geomagnetic field vector can be expressed

in the orbital frame O as [31]

$$\mathbf{B}_O = \frac{\mu_m}{r^3} \begin{bmatrix} \cos nt \sin i_m \\ -\cos i_m \\ 2 \sin nt \sin i_m \end{bmatrix}, \quad (4.9)$$

where i_m is the inclination of the spacecraft's orbit with respect to the magnetic equator, R is the orbital radius, and μ_m is the total dipole strength of the Earth, which is approximately 10^{16} Wb · m. Time is measured from $t = 0$ at the ascending-node crossing of the magnetic equator. Clearly, the Earth's magnetic field in the Body frame B can be obtained using the attitude matrix \mathbf{R} as

$$\mathbf{B} = \mathbf{R} \mathbf{B}_O. \quad (4.10)$$

In this thesis, we consider a small satellite that has a circular at a low altitude. We assume that the control objective is to achieve three-axis stabilized nadir-pointing attitude for the satellite. Since the orientation of the satellite is described relative to the orbital reference frame O . when the attitude of the satellite is the identity ($\mathbf{R} = \mathbf{I}$), the body-fixed xyz axes coincide with the orbital $x_o y_o z_o$ axes. Since the strength of the Earth's magnetic field at this low Earth orbit (LEO) is relatively significant, magnetic torquers can be used to achieve global attitude control.

We will consider to different orbits: a near-magnetic-polar orbit ($i_m \cong 90^\circ$) and a 60° inclination orbit. Let $\mathbf{M} = \tilde{\mathbf{B}} \mathbf{u}$, where $\tilde{\mathbf{B}}$ is the skew symmetric matrix corresponding to the magnetic field vector \mathbf{B} . Then, the magnetic torque vector can be expressed in terms of the new control vector \mathbf{u} as

$$\boldsymbol{\tau} = \mathbf{G}(t) \mathbf{u}, \quad (4.11)$$

where

$$\mathbf{G}(t) = \tilde{\mathbf{B}} \tilde{\mathbf{B}}^T = \mathbf{R} \tilde{\mathbf{B}}_O \tilde{\mathbf{B}}_O^T \mathbf{R}^T.$$

Using the fact that

$$\tilde{\mathbf{B}}_O \tilde{\mathbf{B}}_O^T = \mathbf{B}_O^T \mathbf{B}_O \mathbf{I} - \mathbf{B}_O \mathbf{B}_O^T,$$

we can compute $\mathbf{G}(t)$ for polar orbit as

$$\mathbf{G}(t) = \frac{\mu_m^2}{r^6} \mathbf{R} \begin{bmatrix} 4 \sin^2 nt & 0 & -\sin 2nt \\ 0 & 1 + 3 \sin^2 nt & 0 \\ -\sin 2nt & 0 & \cos^2 nt \end{bmatrix} \mathbf{R}^T, \quad (4.12)$$

and for 60° orbit as

$$\mathbf{G}(t) = \frac{\mu_m^2}{r^6} \mathbf{R} \begin{bmatrix} 3 \sin^2 nt + 0.25 & 0.25\sqrt{3} \cos nt & -0.75 \sin 2nt \\ 0.25\sqrt{3} \cos nt & 0.75(1 + 3 \sin^2 nt) & 0.5\sqrt{3} \sin nt \\ -0.75 \sin 2nt & 0.5\sqrt{3} \sin nt & 0.75 \cos^2 nt + 0.25 \end{bmatrix} \mathbf{R}^T. \quad (4.13)$$

Chapter 5

Feedback Control Laws

In this chapter, we present feedback control laws that achieve three-axis stabilized nadir-pointing attitude. In other words, the control objective is to align the body-fixed reference axes with the orbital reference axes.

5.0.1 Full-State Feedback

The control objective in this paper is to drive the system to the desired state described by the identity quaternion and zero relative angular velocity, i.e. to achieve $\mathbf{q} \rightarrow \pm \mathbf{1}$, where $\mathbf{1}$ denotes the identity quaternion whose vector part is zero and scalar part is unity, and $\boldsymbol{\omega} \rightarrow \boldsymbol{\omega}_o$. Note that for any quaternion \mathbf{q} , $+\mathbf{q}$ and $-\mathbf{q}$ correspond to physically the same orientation. To achieve this control objective, we modify the control law in [17] as

$$\boldsymbol{\tau} = -\mathbf{G}(t) [\epsilon^2 k_1 \mathbf{q}_v + \epsilon k_2 (\boldsymbol{\omega} + n \mathbf{r}_y)] , \quad (5.1)$$

where k_1 and k_2 are positive gains and ϵ is a sufficiently small positive parameter.

Following the development in [17], we employ averaging based arguments to prove

that the control law (5.1) achieves the control objective for sufficiently large values of gains. Define the new coordinates

$$\boldsymbol{\eta}_1 = \mathbf{q}_v, \quad \boldsymbol{\eta}_2 = \frac{\boldsymbol{\omega} + n\mathbf{r}_y}{\epsilon}$$

so that the orbit averaged closed-loop system can be expressed as

$$\dot{\boldsymbol{\eta}}_1 = \frac{\epsilon}{2}(q_4\mathbf{I} + \tilde{\boldsymbol{\eta}}_1)\boldsymbol{\eta}_2, \quad (5.2)$$

$$\dot{q}_4 = -\frac{\epsilon}{2}\boldsymbol{\eta}_1^T \boldsymbol{\eta}_2, \quad (5.3)$$

$$\dot{\boldsymbol{\eta}}_2 = -\frac{\epsilon}{J}\bar{\mathbf{G}}(k_1\boldsymbol{\eta}_1 + k_2\boldsymbol{\eta}_2) - \epsilon\bar{n}\tilde{\boldsymbol{\eta}}_2\mathbf{r}_y, \quad (5.4)$$

where $\epsilon\bar{n} = n$ and $\bar{\mathbf{G}}$ is the orbital average of $\mathbf{G}(t)$ given by equation (4.12) for the near-polar orbit and by (4.13) for the 60° inclination orbit. Here, we have used the fact that

$$\dot{\mathbf{r}}_y = -\boldsymbol{\omega} \times \mathbf{r}_y = -(\boldsymbol{\omega} + n\mathbf{r}_y) \times \mathbf{r}_y.$$

Remark: *The orbit average of a slowly varying function $f(nt)$ is defined as*

$$\overline{f(nt)} = \frac{n}{2\pi} \int_0^{2\pi/n} f(nt) dt.$$

Therefore, using the fact that

$$\overline{\sin^2 nt} = \overline{\cos^2 nt} = 0.5, \quad \overline{\sin 2nt} = 0,$$

$\bar{\mathbf{G}}$ can be computed as

$$\bar{\mathbf{G}} = \frac{\mu_m^2}{r^6} \mathbf{R} \begin{bmatrix} \bar{g}_1 & 0 & 0 \\ 0 & \bar{g}_2 & 0 \\ 0 & 0 & \bar{g}_3 \end{bmatrix} \mathbf{R}^T.$$

where $(\bar{g}_1, \bar{g}_2, \bar{g}_3) = (2, 2.5, 0.5)$ for a near-polar orbit and $(\bar{g}_1, \bar{g}_2, \bar{g}_3) = (7/4, 15/8, 5/8)$ for a 60°-inclination orbit.

Proposition 1: *Consider the isoinertial spacecraft described by (4.4) and (4.6) with the magnetic torque law (5.1). Assume that*

$$k_2 > (\bar{g}_3^{-1} - \bar{g}_1^{-1}) J \bar{n} \frac{r^6}{\mu_m^2}. \quad (5.5)$$

Then, there exists an $\epsilon^ > 0$ such that for $0 < \epsilon < \epsilon^*$ the control law (5.1) achieves asymptotic attitude regulation of the spacecraft.*

Proof: Consider the orbit averaged closed-loop system (5.2)-(5.4) and assume that the condition (5.5) is satisfied. Let

$$V = k_1 \boldsymbol{\eta}_1^T \boldsymbol{\eta}_1 + k_1 (q_4 - 1)^2 + \frac{1}{2} J \boldsymbol{\eta}_2^T \bar{\mathbf{G}}^{-1} \boldsymbol{\eta}_2$$

be a candidate Lyapunov function. Then, taking the time derivative along the closed-loop trajectories yields

$$\begin{aligned} \dot{V} &= 2k_1 \boldsymbol{\eta}_1^T \dot{\boldsymbol{\eta}}_1 + 2k_1 (q_4 - 1) \dot{q}_4 + J \boldsymbol{\eta}_2^T \bar{\mathbf{G}}^{-1} \dot{\boldsymbol{\eta}}_2 \\ &= -\epsilon k_2 \boldsymbol{\eta}_2^T \boldsymbol{\eta}_2 - \epsilon J \bar{n} \boldsymbol{\eta}_2^T \bar{\mathbf{G}}^{-1} \tilde{\boldsymbol{\eta}}_2 \mathbf{r}_y \\ &= -\epsilon \boldsymbol{\eta}_2^T (k_2 + (\bar{g}_3^{-1} - \bar{g}_1^{-1}) J \bar{n} \frac{R^6}{\mu_m^2} r_z r_x^T) \boldsymbol{\eta}_2 \leq 0. \end{aligned}$$

Here, we have used the fact that

$$\mathbf{R}^T (\boldsymbol{\eta}_2 \times \mathbf{r}_y) = \mathbf{R}^T \boldsymbol{\eta}_2 \times \mathbf{R}^T \mathbf{r}_y$$

and that the 2-norm of $r_z r_x^T$ is unity.

Now, it suffices to show that \dot{V} is not identically zero along any solutions of (5.2)-

(5.4) other than the desired equilibrium. By LaSalle's invariance principle $\boldsymbol{\eta}_1$ and $\boldsymbol{\eta}_2$ will converge to the largest invariant subset of $\{(\boldsymbol{\eta}_1, \boldsymbol{\eta}_2) \mid \dot{V} = 0\}$. On the set, $\boldsymbol{\eta}_2 \equiv 0 \Rightarrow \dot{\boldsymbol{\eta}}_2 \equiv 0$, which implies $\boldsymbol{\eta}_1 = 0$ and $q_4 \rightarrow \pm 1$. Therefore, the averaged system is exponentially stable at the identity quaternion and zero relative angular velocity (i.e. $\mathbf{q} \rightarrow \pm \mathbf{1}$ and $\boldsymbol{\omega} \rightarrow \boldsymbol{\omega}_o$). According to the generalized averaging theory [11], since the averaged system is exponentially stable, there exists an $\epsilon^* > 0$ such that for $0 < \epsilon < \epsilon^*$ the control law (5.1) achieves asymptotic attitude regulation of the spacecraft.

5.0.2 Passivity-Based Feedback

For small satellites, the ability of three-axis stabilization without angular velocity measurement is especially important since it eliminates the need for rate sensors. The dependence of the control law on velocity information can be eliminated using passivity techniques [16, 28].

Combining the ideas in [15, 17], we propose the following quaternion feedback law:

$$\boldsymbol{\tau} = -\mathbf{G}(t) [\epsilon^2 k_1 \mathbf{q}_v + \epsilon k_2 (q_4 \mathbf{y}_v - y_4 \mathbf{q}_v - \tilde{\mathbf{q}}_v \mathbf{y}_v)] , \quad (5.6)$$

$$\dot{\boldsymbol{\alpha}} = -\boldsymbol{\alpha} + \mathbf{q} , \quad (5.7)$$

$$\mathbf{y} = -\boldsymbol{\alpha} + \mathbf{q} , \quad (5.8)$$

where k_1 and k_2 are positive gains, ϵ is a sufficiently small positive parameter; and $\boldsymbol{\alpha} = [\boldsymbol{\alpha}_v^T, \alpha_4]^T \in \mathfrak{R}^4$ and $\mathbf{y} = [\mathbf{y}_v^T, y_4]^T \in \mathfrak{R}^4$ are the filter state and output vectors, respectively.

Again as in [17], we can use a generalized averaging procedure to show that there exists an $\epsilon^* > 0$ such that for $0 < \epsilon < \epsilon^*$ the passivity-based control law (5.6)-(5.8) achieves asymptotic attitude regulation of the spacecraft.

Chapter 6

Simulation Results

6.1 Simulation Results Using the IGRF Model

This section illustrates the effectiveness of the magnetic stabilization techniques described in the previous chapter through computer simulations. We consider a picosatellite at a circular orbit of radius 7000 km, so that the orbital rate is $n=0.00108$ rad/s. The satellite-fixed xyz -axes are chosen to be the principal axes. The principal moments of inertia are given as

$$J_x = J_y = J_z = J = 1/600 \text{ kg} \cdot \text{m}^2.$$

6.1.1 Full-State Feedback

A computer implementation of the control law given by (5.1) with the control parameters $\epsilon = 0.0005$, $k_1 = k_2 = 10^7$ was used to achieve three-axis stabilized nadir-pointing attitude, i.e. to drive the system to the desired state described by the identity quater-

nion and zero relative angular velocity. Note that since

$$k_2 = 10^7 > (\bar{g}_3^{-1} - \bar{g}_1^{-1}) J \bar{n} \frac{r^6}{\mu_m^2},$$

the condition (5.5) is satisfied for both the 60°-inclination orbit and the near polar orbit. The torque coils were turned off for 1 second for geomagnetic field measurements after every 9 seconds of magnetic torquing (i.e., applying a 90% duty cycle). The results of the computer simulation for a sample initial condition given by $(q_1, q_2, q_3, q_4) = (0.5, 0.5, 0.5, 0.5)$ and $(\omega_1, \omega_2, \omega_3) = (0.1, 0.1, 0.1)$ rad/s are shown in Figures 6.1-6.3 for the 60°-inclination orbit and in Figures 6.4-6.6 for the near-polar orbit. It can be seen that the desired state is achieved in about 7 orbits while the magnitudes of dipole moments of the magnetic coils about the xyz -axes do not exceed $0.02 \text{ A} \cdot \text{m}^2$.

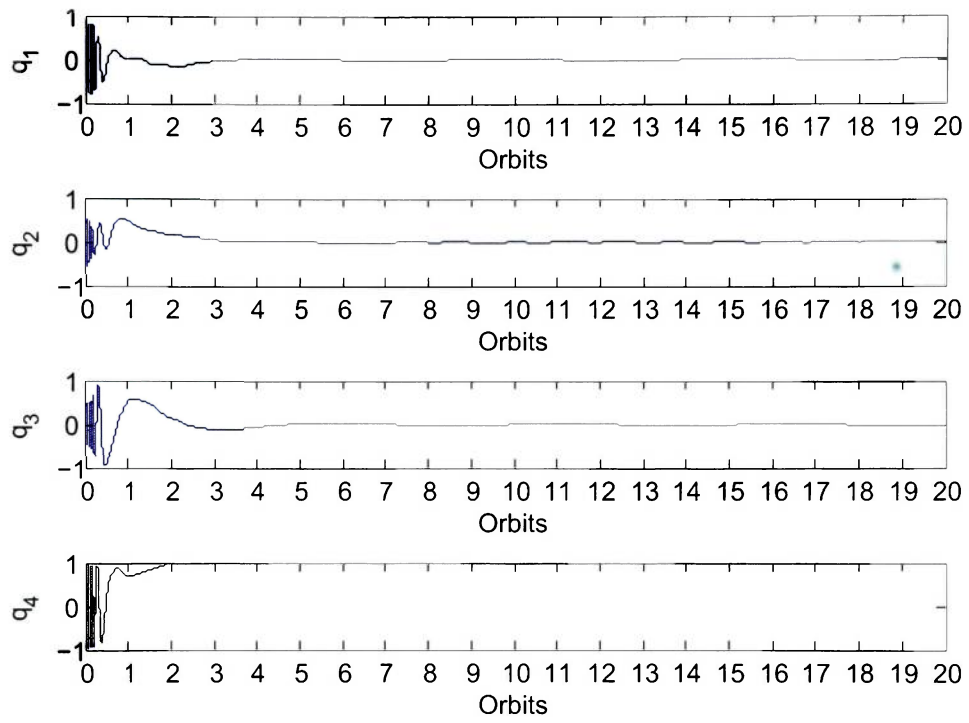


Figure 6.1: Quaternions for $i_m = 60^\circ$ (Full-State Feedback).

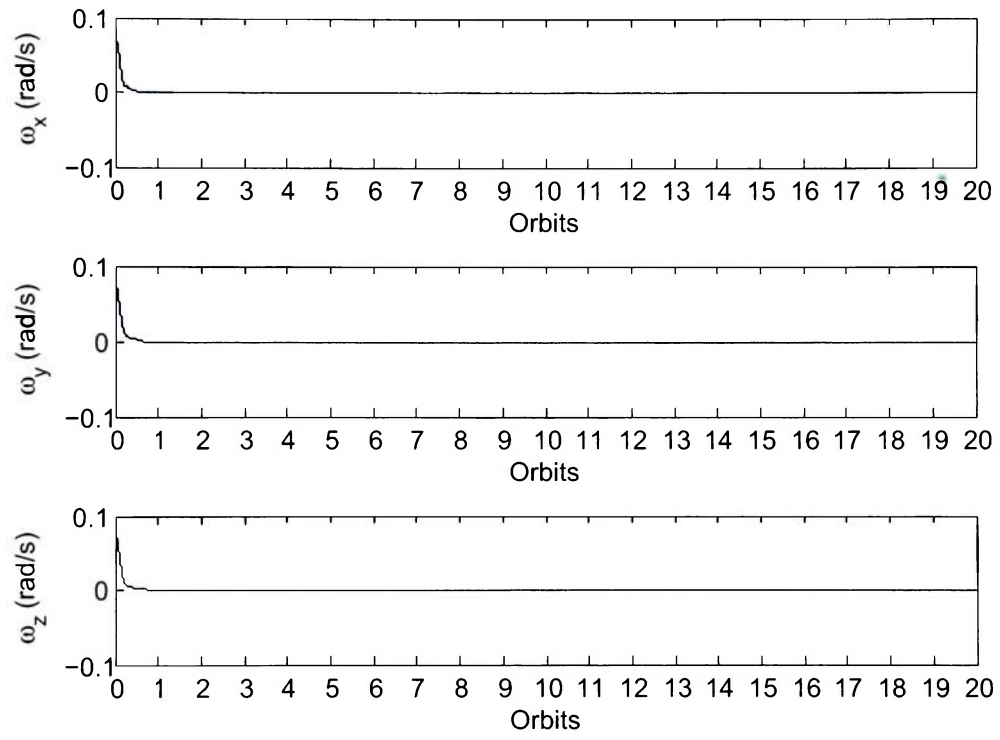


Figure 6.2: Angular Rates for $i_m = 60^\circ$ (Full-State Feedback).

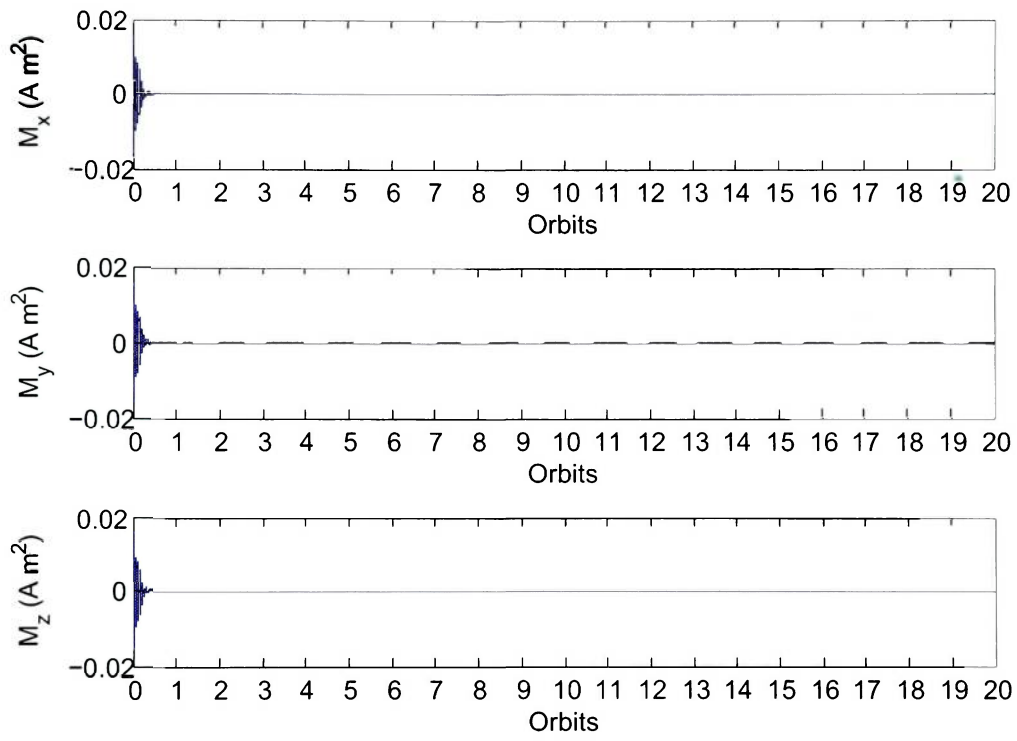


Figure 6.3: Magnetic Dipole Moments for $i_m = 60^\circ$ (Full-State Feedback).

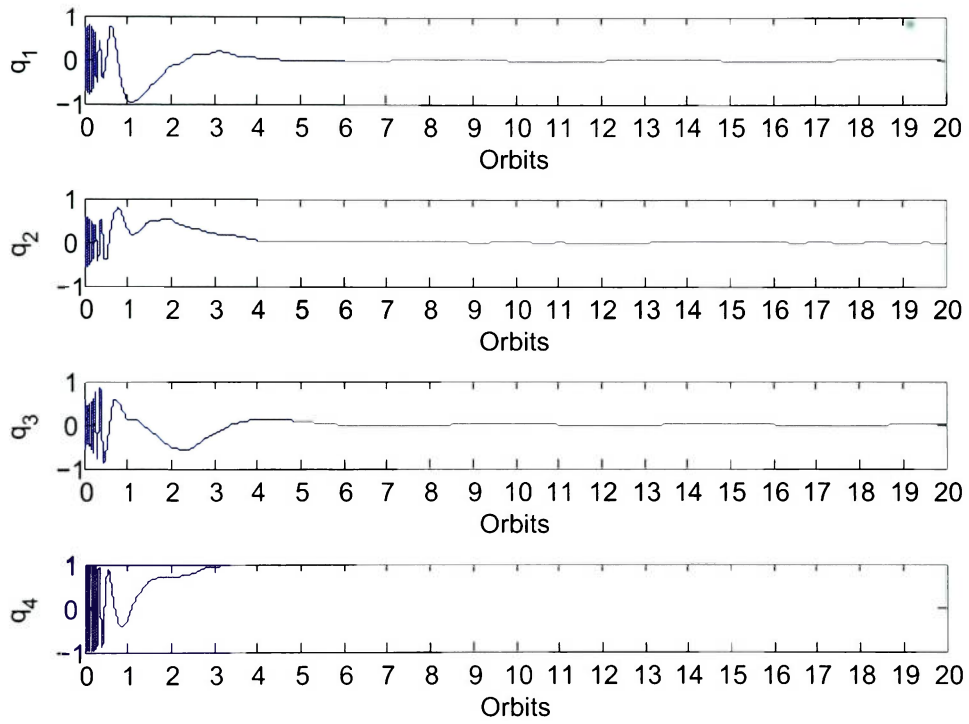


Figure 6.4: Quaternions for $i_m = 90^\circ$ (Full-State Feedback).

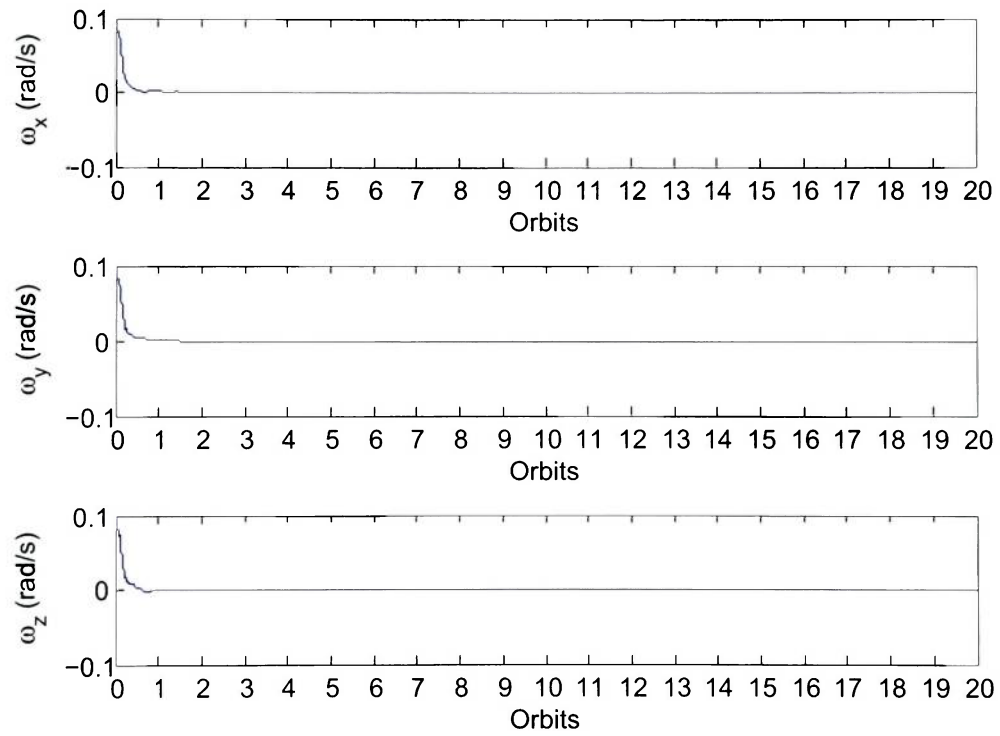


Figure 6.5: Angular Rates for $i_m = 90^\circ$ (Full-State Feedback).

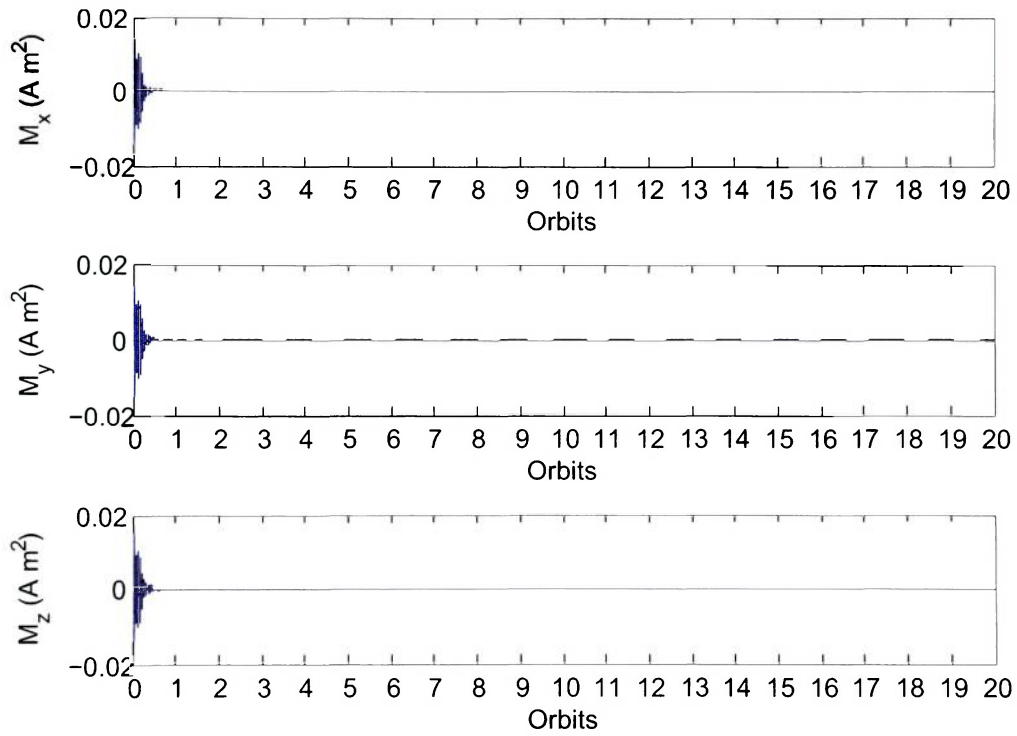


Figure 6.6: Magnetic Dipole Moments for $i_m = 90^\circ$ (Full-State Feedback).

6.1.2 Passivity-Based Feedback

We next consider a computer implementation of the control law given by (5.6)-(5.8) with the same control parameters as in the full-state feedback case. Again the torque coils were turned off for 1 second for geomagnetic field measurements after every 9 seconds of magnetic torquing. Figures 6.7-6.9 and 6.10-6.12 (for the 60°-inclination and 90°-inclination orbits, respectively) show the results of the simulation for the same sample initial condition given by $(q_1, q_2, q_3, q_4) = (0.5, 0.5, 0.5, 0.5)$ and $(\omega_1, \omega_2, \omega_3) = (0.1, 0.1, 0.1)$ rad/s. It can be seen that the desired state is achieved in about 12 orbits and the magnitudes of dipole moments of the magnetic coils about the xyz -axes do not exceed $0.01 \text{ A} \cdot \text{m}^2$.

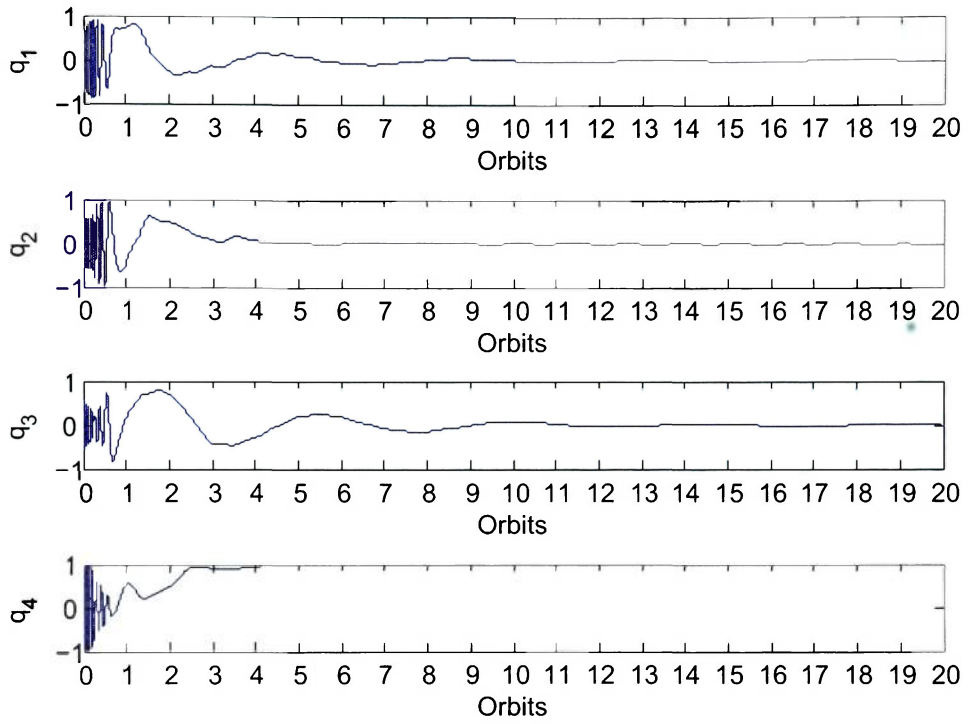


Figure 6.7: Quaternions for $i_m = 60^\circ$ (Passivity-Based Feedback).

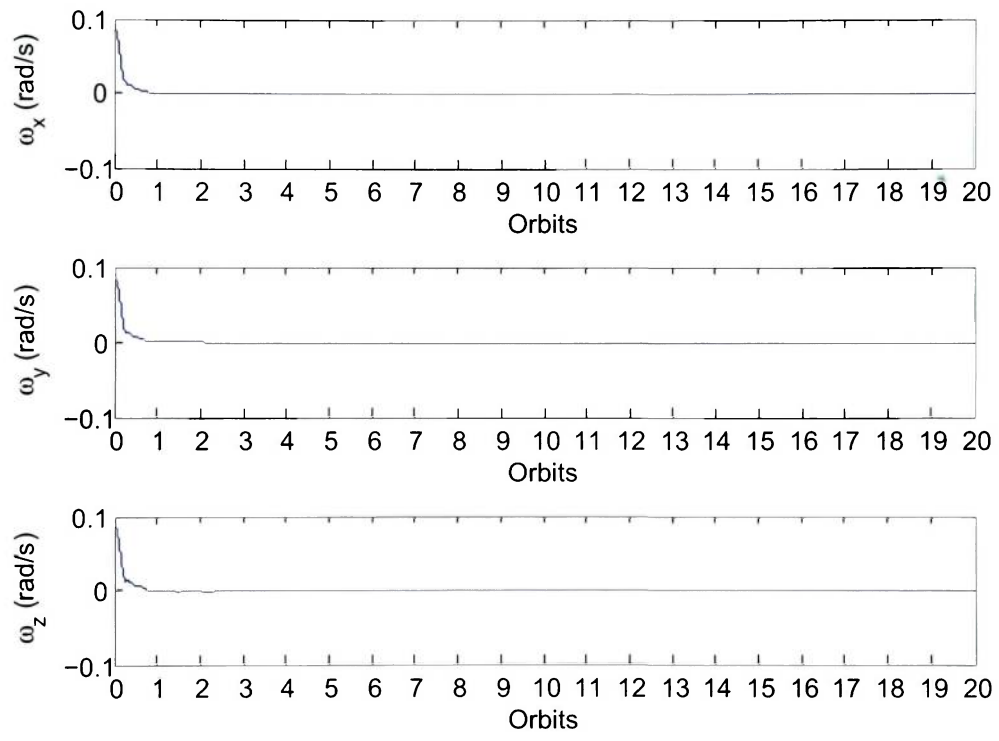


Figure 6.8: Angular Rates for $i_m = 60^\circ$ (Passivity-Based Feedback).

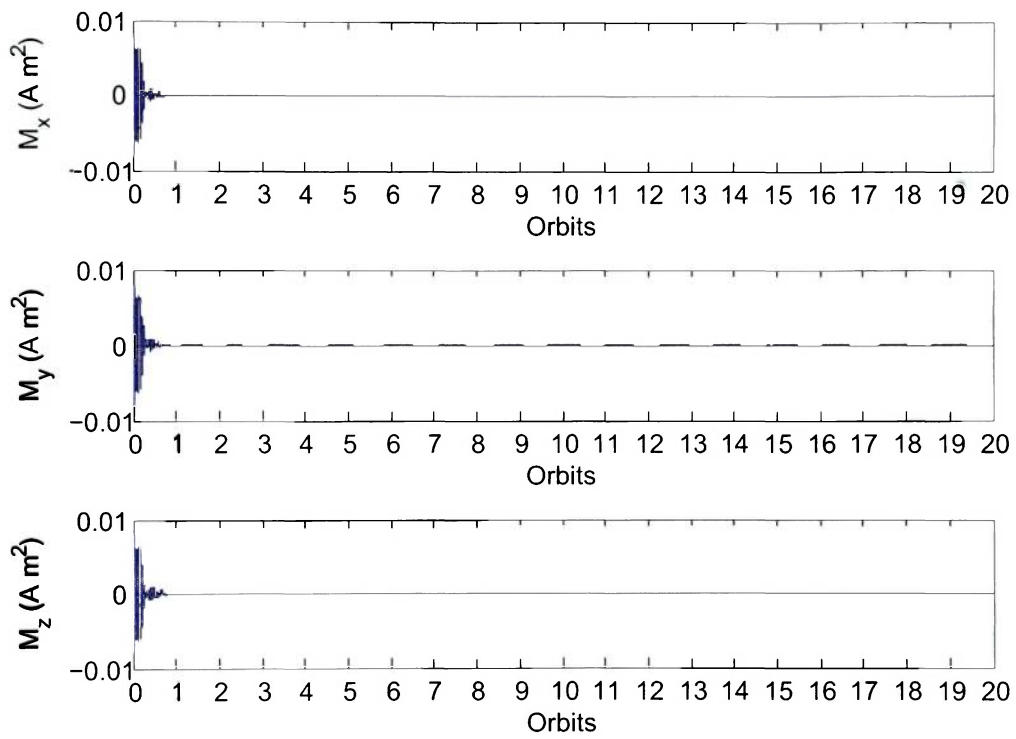


Figure 6.9: Magnetic Dipole Moments for $i_m = 60^\circ$ (Passivity-Based Feedback).

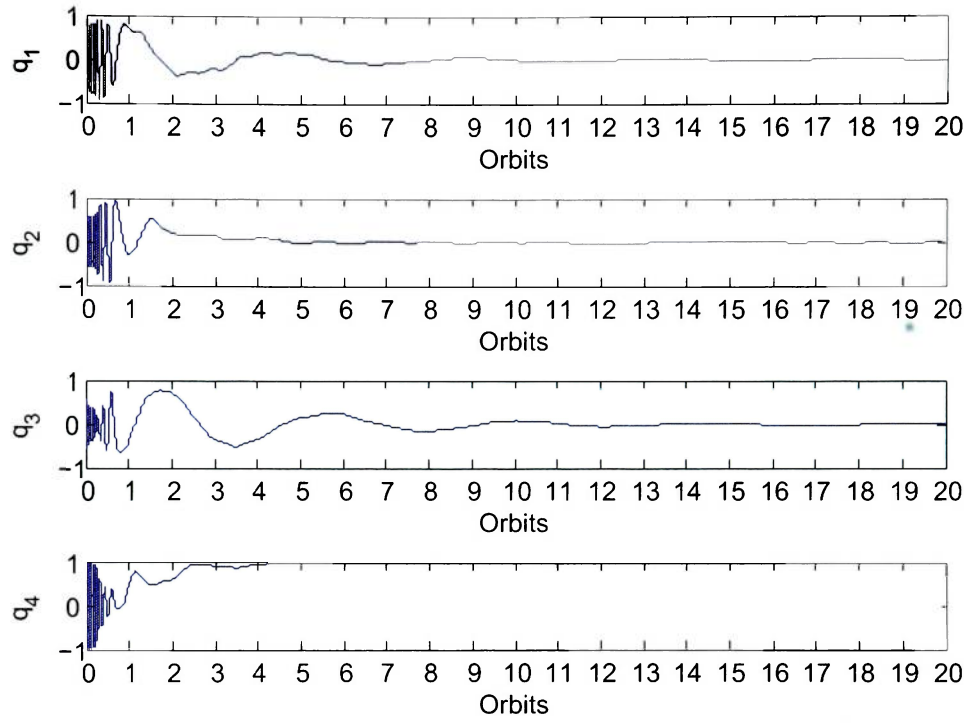


Figure 6.10: Quaternions for $i_m = 90^\circ$ (Passivity-Based Feedback).

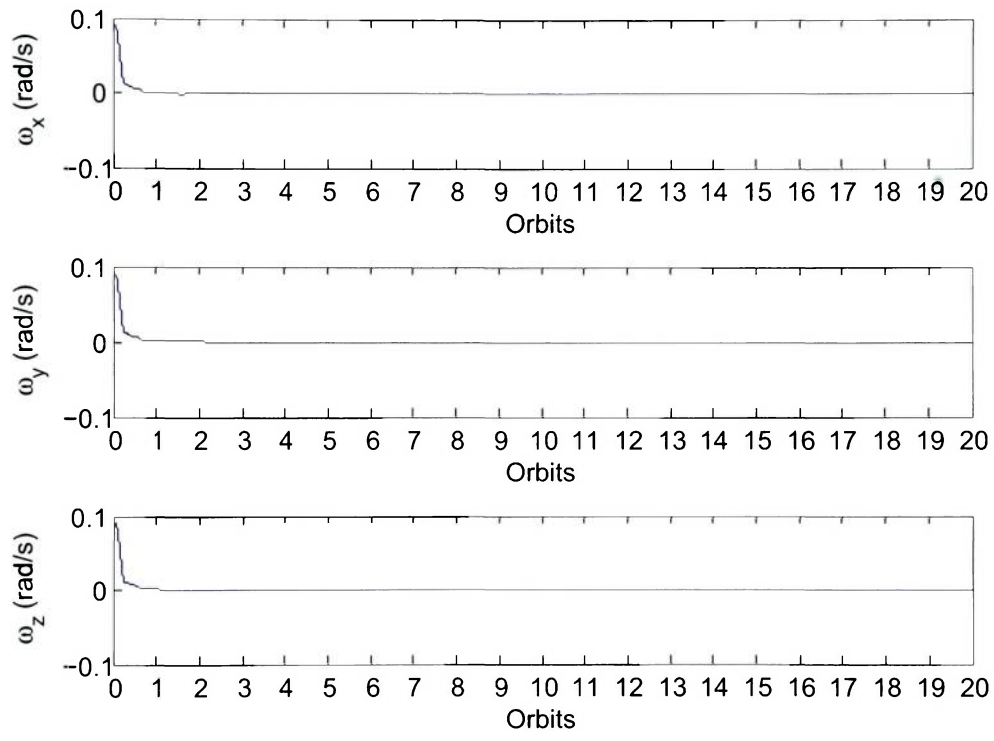


Figure 6.11: Angular Rates for $i_m = 90^\circ$ (Passivity-Based Feedback).

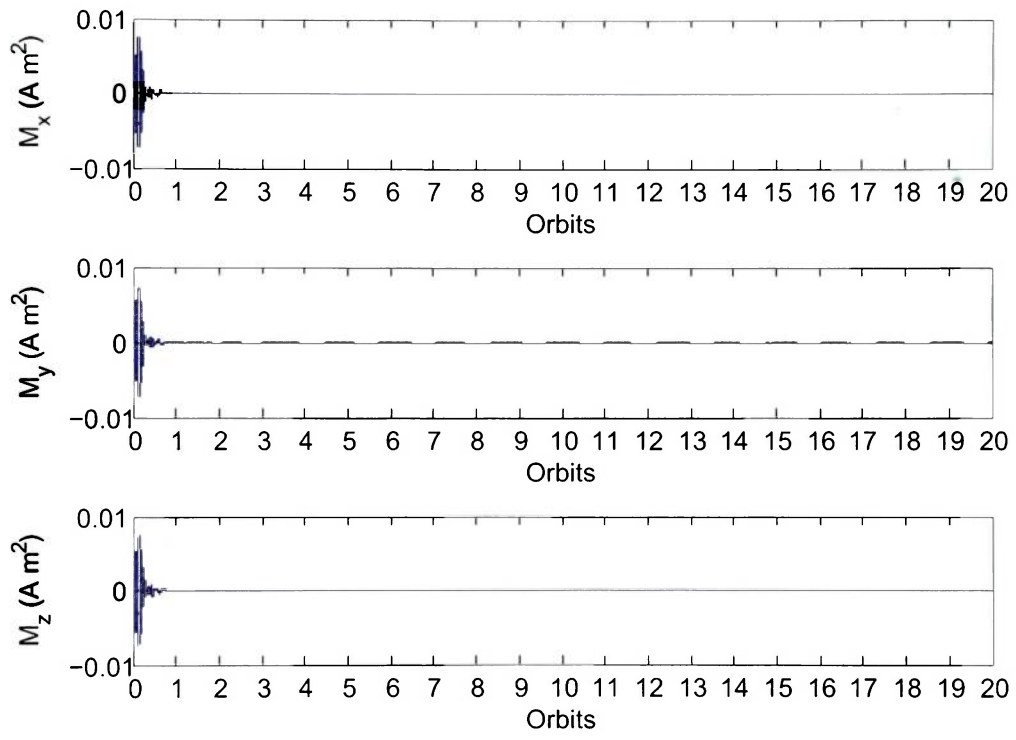


Figure 6.12: Magnetic Dipole Moments for $i_m = 90^\circ$ (Passivity-Based Feedback).

6.2 Simulation Results for the Tilted Dipole Model

6.2.1 Full-State Feedback

A computer implementation of the control law given by (5.1) with the control parameters $\epsilon = 0.0005$, $k_1 = k_2 = 10^7$ was used to achieve three-axis stabilized nadir-pointing attitude, i.e. to drive the system to the desired state described by the identity quaternion and zero relative angular velocity. Note that since

$$k_2 = 10^7 > (\bar{g}_3^{-1} - \bar{g}_1^{-1}) J \bar{n} \frac{r^6}{\mu_m^2},$$

the condition (5.5) is satisfied for both the 60° -inclination orbit and the near polar orbit. The torque coils were turned off for 1 second for geomagnetic field measurements after every 9 seconds of magnetic torquing (i.e., applying a 90% duty cycle). The results of the computer simulation for a sample initial condition given by $(q_1, q_2, q_3, q_4) = (0.5, 0.5, 0.5, 0.5)$ and $(\omega_1, \omega_2, \omega_3) = (0.1, 0.1, 0.1)$ rad/s are shown in Figures 6.13-6.15 for the 60° -inclination orbit and in Figures 6.16-6.18 for the near-polar orbit. It can be seen that the desired state is achieved in about 6 orbits while the magnitudes of dipole moments of the magnetic coils about the xyz -axes do not exceed $0.02 \text{ A} \cdot \text{m}^2$.

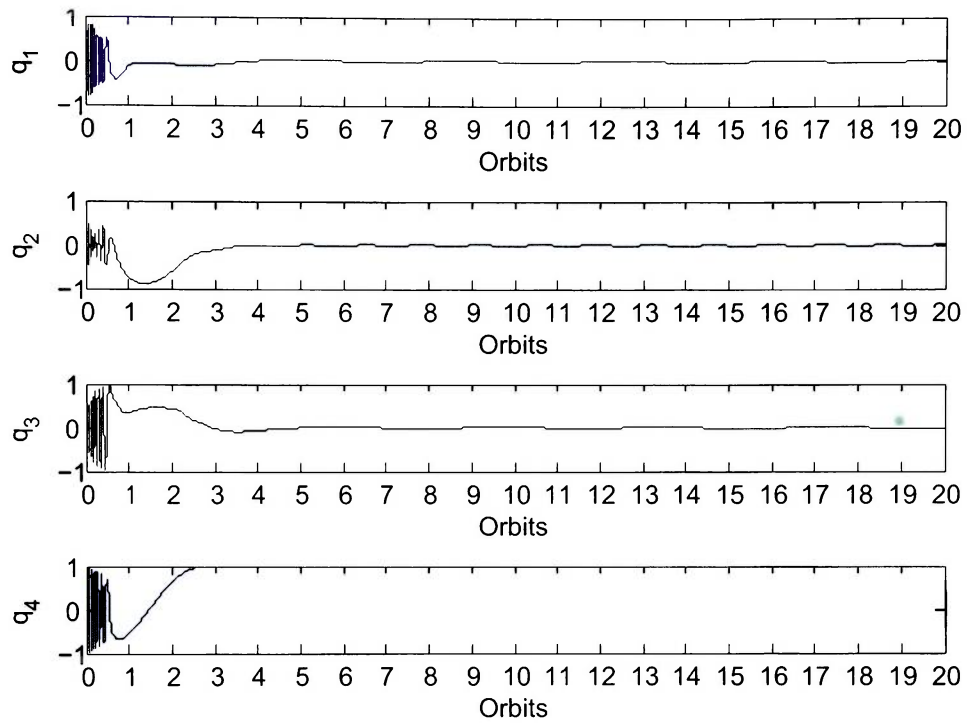


Figure 6.13: Quaternions for $i_m = 60^\circ$ (Full-State Feedback).

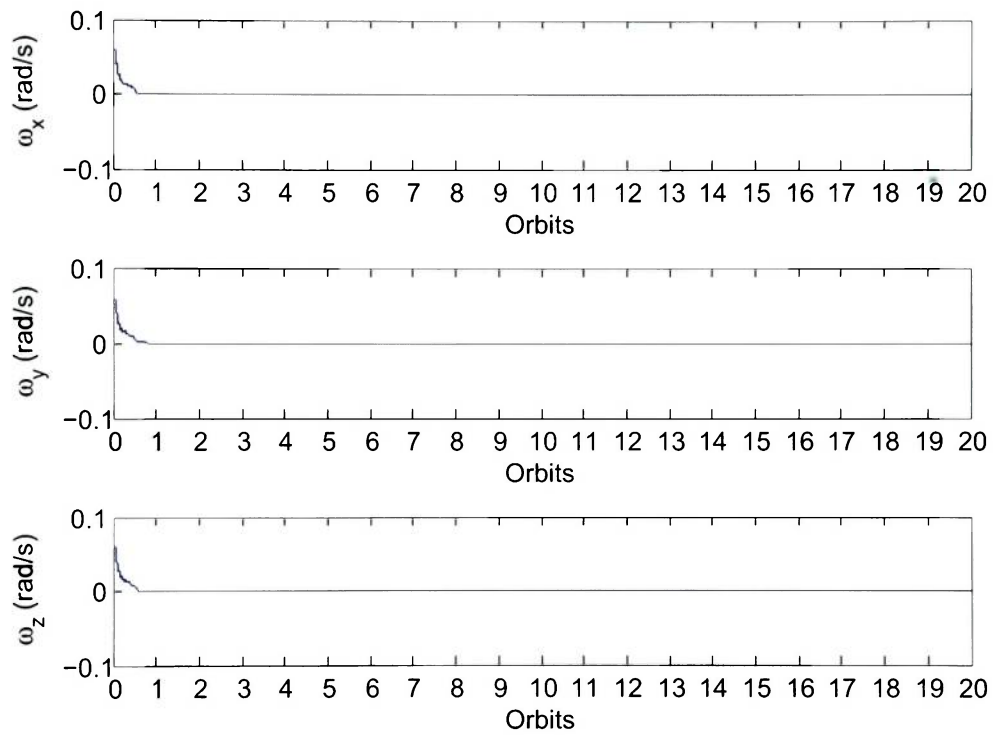


Figure 6.14: Angular Rates for $i_m = 60^\circ$ (Full-State Feedback).

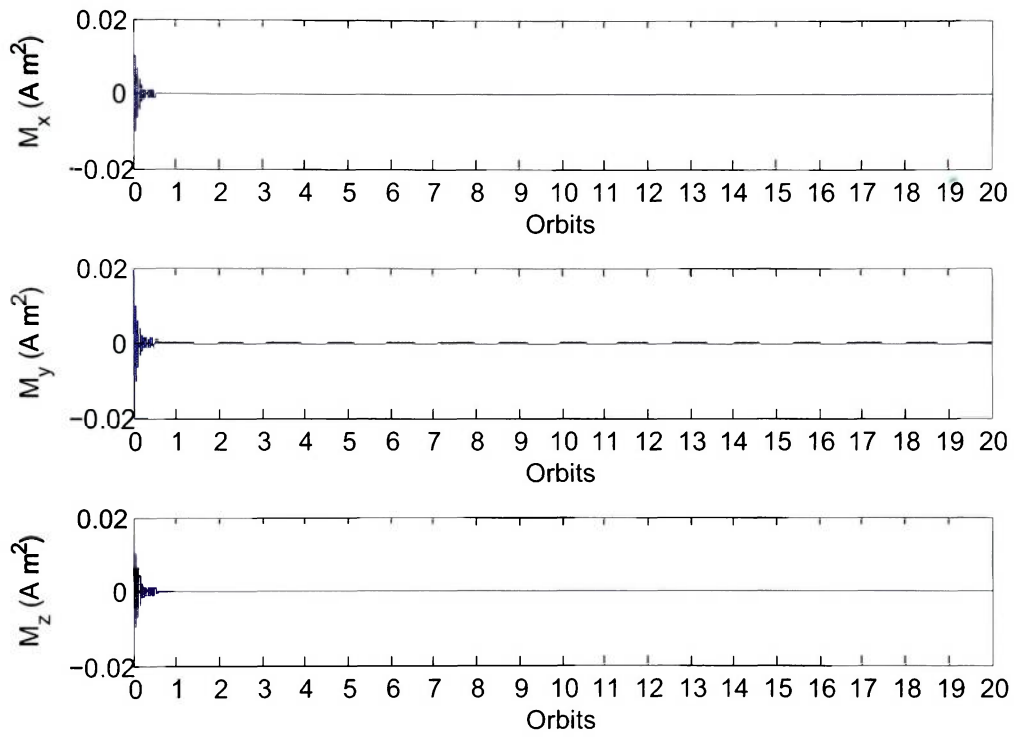


Figure 6.15: Magnetic Dipole Moments for $i_m = 60^\circ$ (Full-State Feedback).

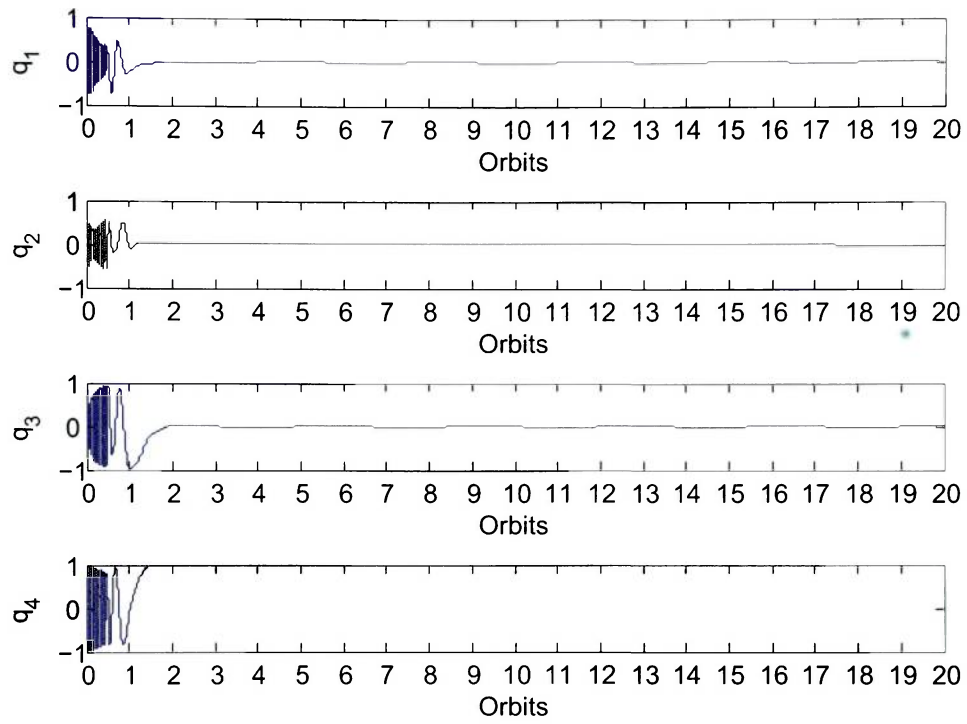


Figure 6.16: Quaternions for $i_m = 90^\circ$ (Full-State Feedback).

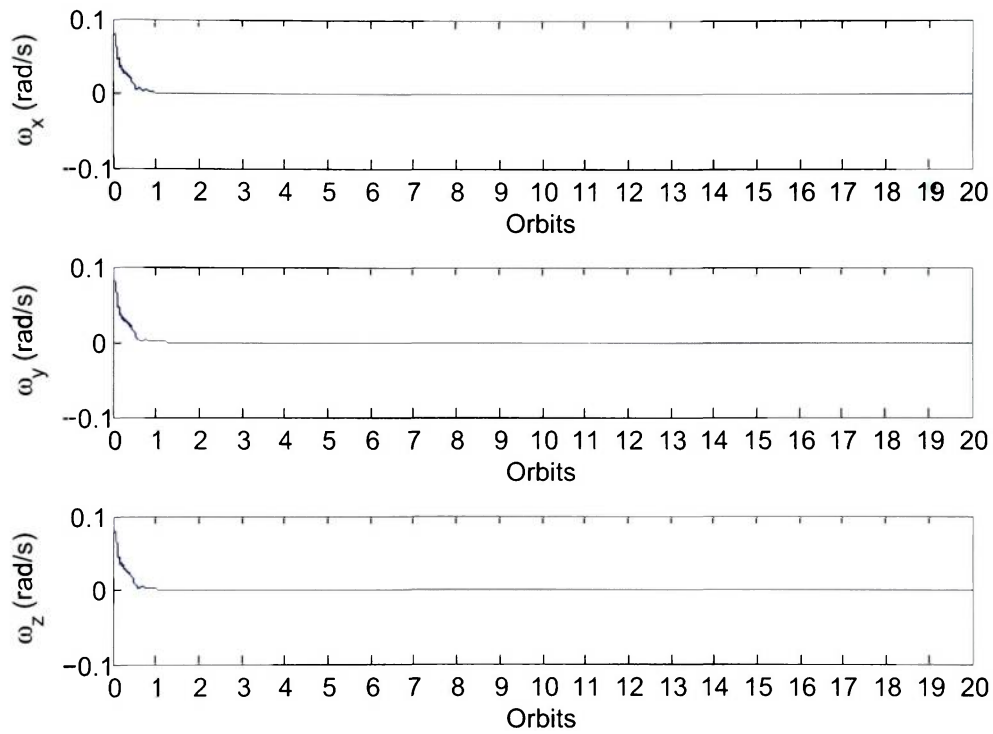


Figure 6.17: Angular Rates for $i_m = 90^\circ$ (Full-State Feedback).

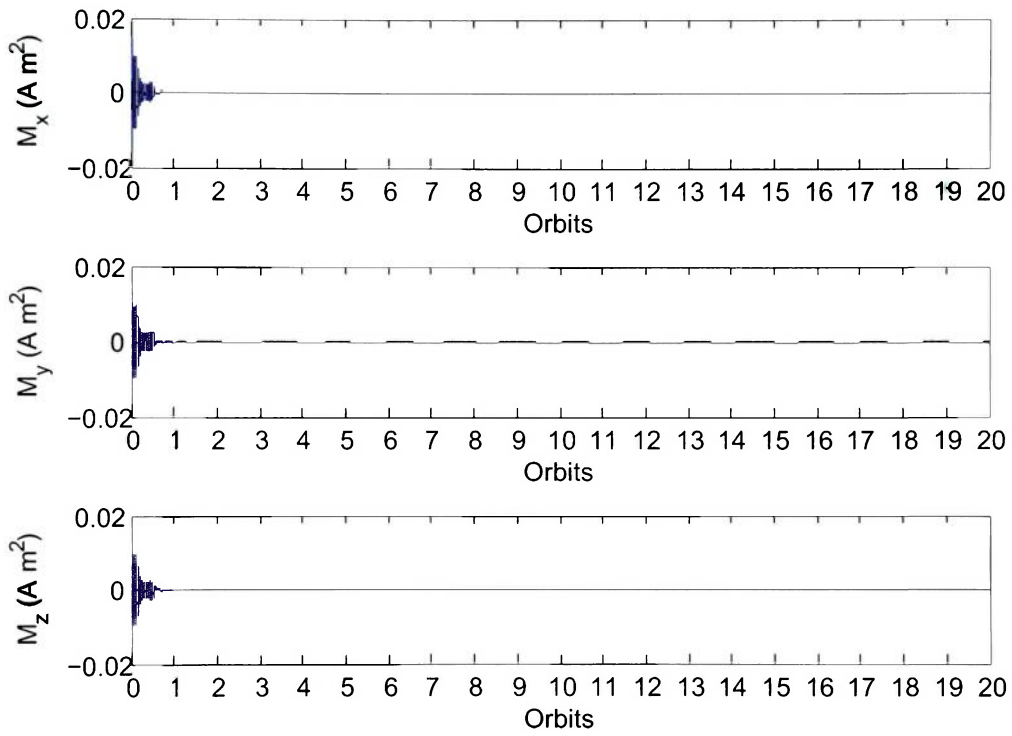


Figure 6.18: Magnetic Dipole Moments for $i_m = 90^\circ$ (Full-State Feedback).

6.2.2 Passivity-Based Feedback

We next consider a computer implementation of the control law given by (5.6)-(5.8) with the same control parameters as in the full-state feedback case. Again the torque coils were turned off for 1 second for geomagnetic field measurements after every 9 seconds of magnetic torquing. Figures 6.19-6.21 and 6.22-6.24 (for the 60°-inclination and 90°-inclination orbits, respectively) show the results of the simulation for the same sample initial condition given by $(q_1, q_2, q_3, q_4) = (0.5, 0.5, 0.5, 0.5)$ and $(\omega_1, \omega_2, \omega_3) = (0.1, 0.1, 0.1)$ rad/s. It can be seen that the desired state is achieved in about 12 orbits and the magnitudes of dipole moments of the magnetic coils about the xyz -axes do not exceed $0.01 \text{ A} \cdot \text{m}^2$.

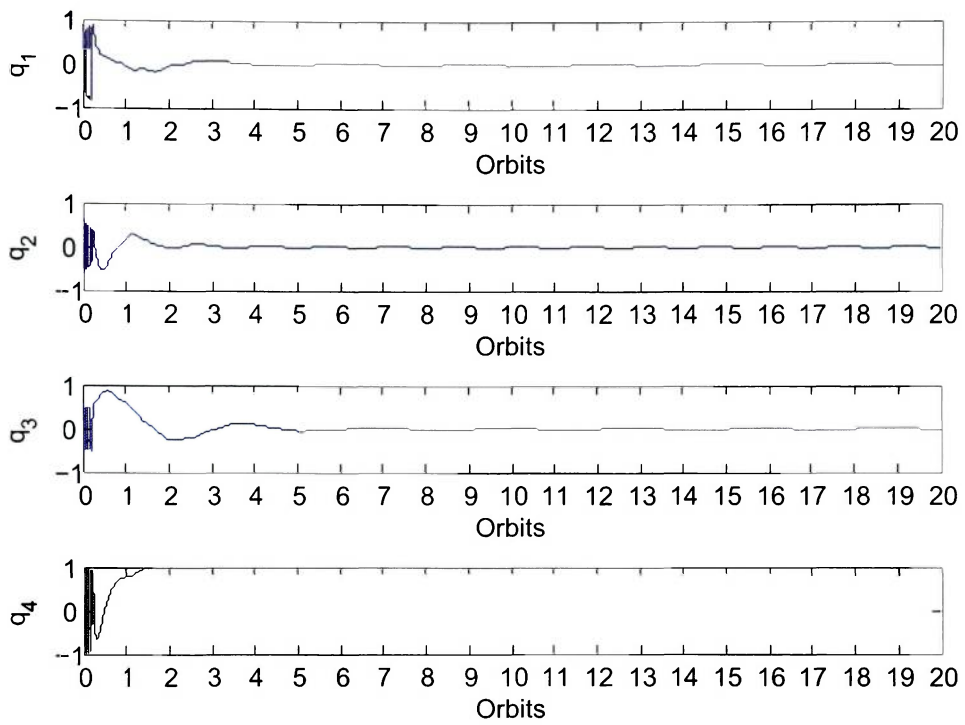


Figure 6.19: Quaternions for $i_m = 60^\circ$ (Passivity-Based Feedback).

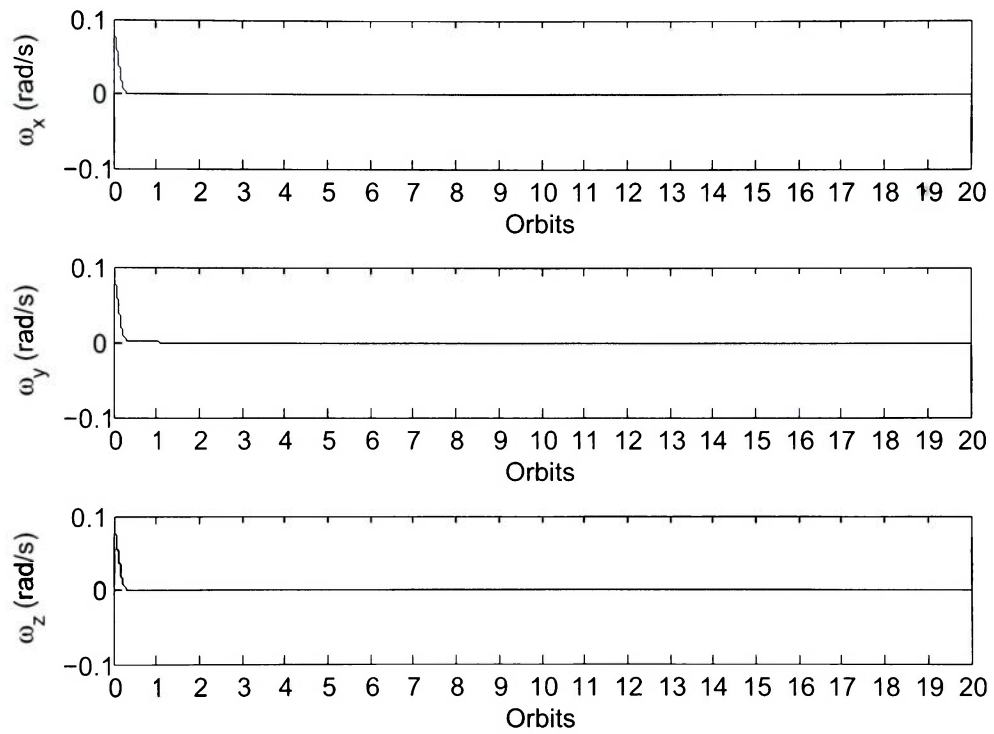


Figure 6.20: Angular Rates for $i_m = 60^\circ$ (Passivity-Based Feedback).

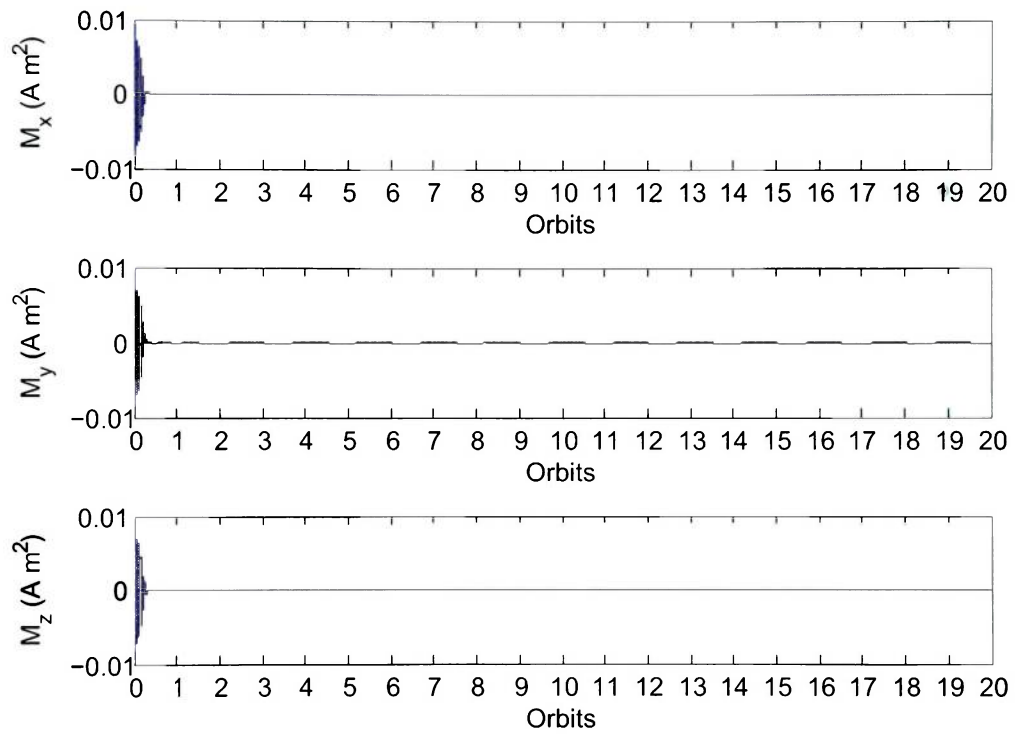


Figure 6.21: Magnetic Dipole Moments for $i_m = 60^\circ$ (Passivity-Based Feedback).

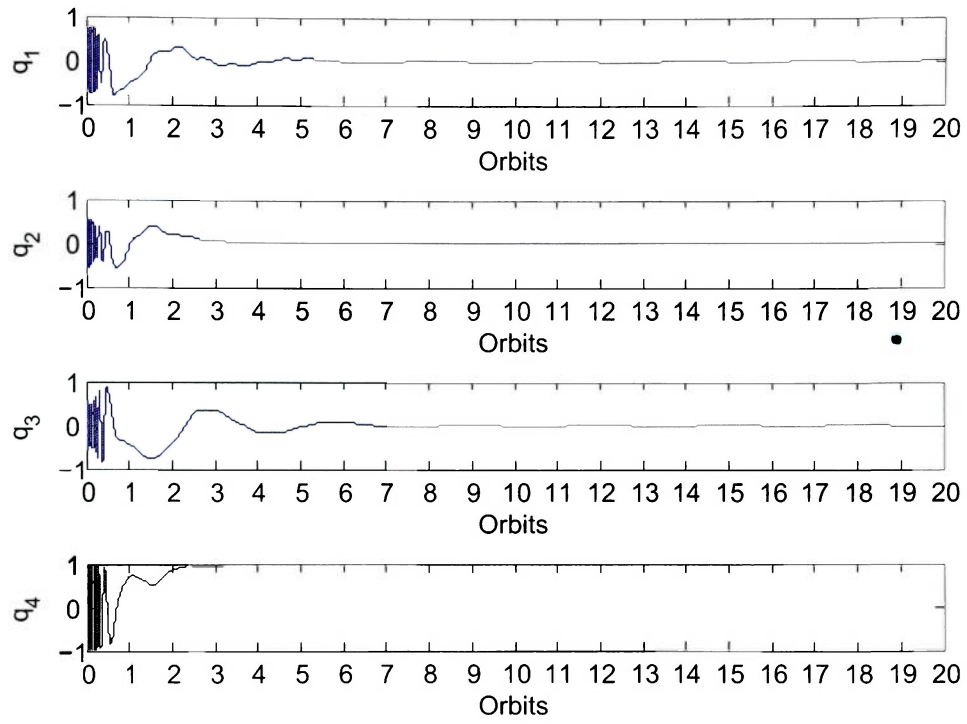


Figure 6.22: Quaternions for $i_m = 90^\circ$ (Passivity-Based Feedback).

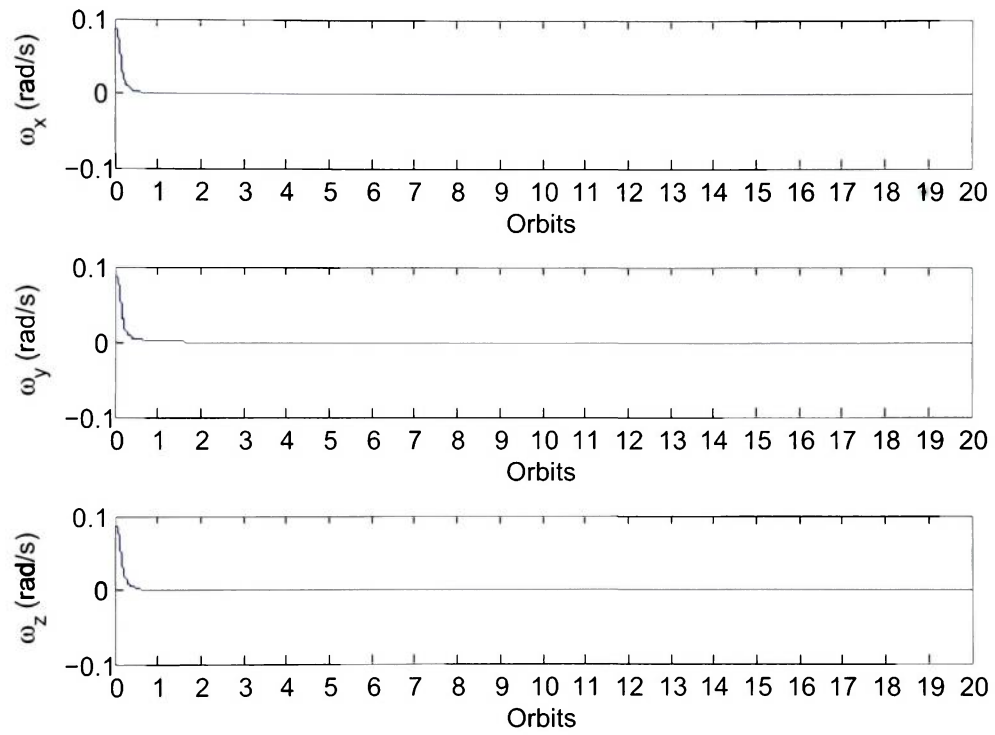


Figure 6.23: Angular Rates for $i_m = 90^\circ$ (Passivity-Based Feedback).

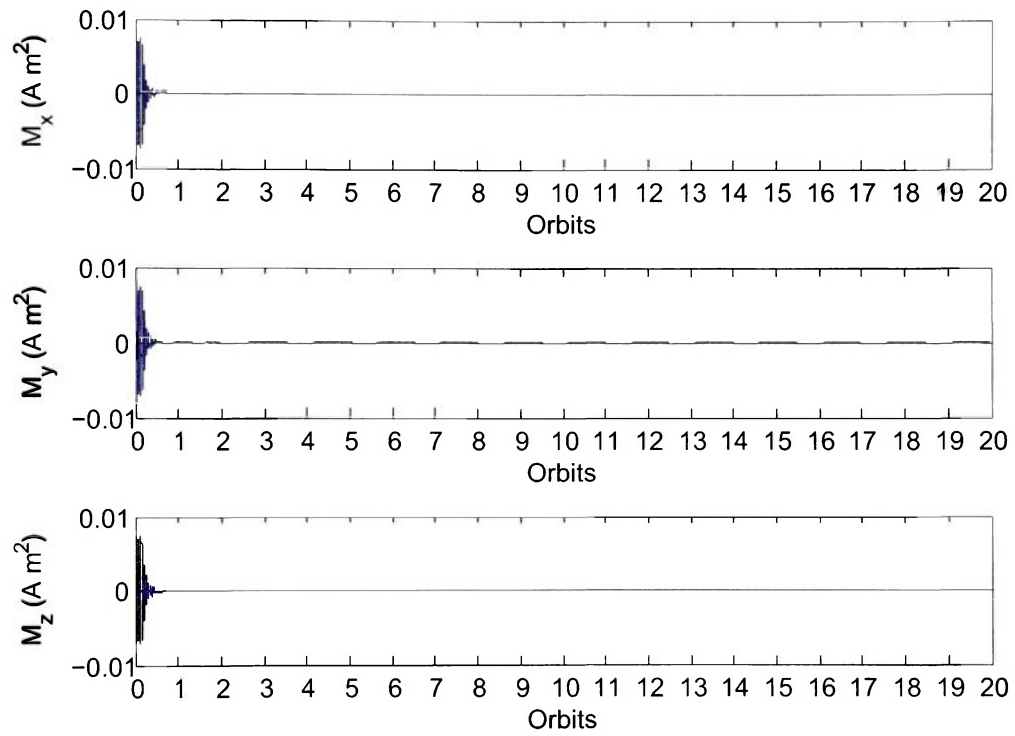


Figure 6.24: Magnetic Dipole Moments for $i_m = 90^\circ$ (Passivity-Based Feedback).

Chapter 7

Conclusions

This thesis has presented two control laws based on averaging for small satellites using magnetic torquers to effectively maneuver the spacecraft for nadir-pointing. The two cases where the controllers are based on are full-state feedback where attitude and angular velocity measurements are used for feedback, and passivity-based feedback where angular velocity are not feedback into the system.

The control laws are demonstrated by running simulations on the tilted dipole model and the IGRF model. The simulations that ran for the IGRF and the tilted dipole model converged approximately on the same number of orbits. The full-state feedback control laws takes around nine to ten orbits to fully converges, while the passivity-based feedback takes eleven to twelve orbits.

Table 7.1: Summary of Simulation Results

B	Case	$i_m = 60^\circ$	$i_m = 90^\circ$
IGRF	Full-state	7	7
Dipole	Full-state	6	5
IGRF	Passivity-based	12	12
Dipole	Passivity-based	7	8

Future research might include design based on sliding mode control since it does

very well at disturbances rejection, however this model requires fast switches. This might cause problem with the dissipation of the current firing into the magnetic coils.

Bibliography

- [1] K. T. Alfriend, "Magnetic attitude control system for dual-spin satellites," *AIAA Journal*, Vol. 13, No. 6, 1975, pp. 817-822.
- [2] C. Arduini and P. Baiocco, "Active magnetic damping attitude control for gravity gradient stabilized spacecraft," *Journal of Guidance, Control, and Dynamics*, Vol. 20, No. 1, 1997, pp. 117-122.
- [3] S. P. Bhat, "Controllability of nonlinear time-varying systems: applications to spacecraft attitude control using magnetic actuation," *IEEE Transactions on Automatic Control*, Vol. 50, No. 11, 2005, pp. 1725-1735.
- [4] A. M. Bloch, M. Reyhanoglu, and N. H. McClamroch, "Control and stabilization of nonholonomic dynamic systems," *IEEE Transactions on Automatic Control*, Vol. 37, No. 11, 1992, pp. 1746-1757.
- [5] C. I. Byrnes and A. Isidori, "On the attitude stabilization of rigid spacecraft," *IFAC Journal Automatica*, Vol. 27, No. 1, 1991, pp. 87-95.
- [6] J. Davis, *Mathematical Modeling of Earth's Magnetic Field*. Technical Note, Virginia Tech, Blacksburg, May 12, 2004.

- [7] R. DeCarlo, S. Zak, and S. V. Drakunov, "Variable structure and sliding mode control," in *The Control Handbook*, CRC Press, Inc., The Electrical Engineering Handbook Series, 1996.
- [8] S. V. Drakunov, "Sliding mode control with multiple equilibrium manifolds," *Proceedings of ME94 International Congress and Exposition (The Winter Annual Meeting of ASME)*, Chicago, IL, Nov. 6-11, 1994, DSC-Vol. 55-1, Dynamic Systems and Control, pp. 101-108.
- [9] P. S. Goel, and S. Rojaram, "Magnetic attitude control of a momentum-biased satellite in near-equatorial orbit," *Journal of Guidance and Control*, Vol. 2, No. 4, 1979, pp. 334-338.
- [10] IAGA V-MOD Geomagnetic Field. *International Geomagnetic Reference Field*, <http://www.ngdc.noaa.gov/IAGA/vmod/igrf.html>.
- [11] H. K. Khalil, *Nonlinear systems*, 3rd Edition, Prentice Hall, 2002.
- [12] H. Krishnan, N. H. McClamroch, and M. Reyhanoglu, "Attitude stabilization of a rigid spacecraft using two momentum wheel actuators," *AIAA Journal of Guidance, Control, and Dynamics*, Vol. 18, No. 2, 1995, pp. 256-263.
- [13] H. Krishnan, M. Reyhanoglu, and N. H. McClamroch, "Attitude stabilization of a rigid spacecraft using two controls: a nonlinear control approach based on spacecraft dynamics," *IFAC Journal Automatica*, Vol. 30, No. 6, 1994, pp. 1023-1027.
- [14] R. Kristianen, *Attitude Control of Microsatellite*. Master's Thesis, Department of Engineering Cybernetics, Norwegian University of Science and Technology, Trondheim. 2000.

- [15] J. Lawton and R. W. Beard, "Model independent eigenaxis maneuvers using quaternion feedback," *Proceedings of the American Control Conference*, 2001, pp. 2339-2344.
- [16] F. Lizarralde and J. Wen, "Attitude control without velocity measurement: A passivity approach," *IEEE Transactions on Automatic Control*, Vol. 41, 1996, pp. 468-472.
- [17] M. Lovera and A. Astolfi, "Spacecraft attitude control using magnetic actuators," *IFAC Journal Automatica*, Vol. 40, 2004, pp. 1405-1414.
- [18] K. L. Makovec, *Satellite attitude control using only electromagnetic actuation*, M.S. Thesis, Virginia Polytechnic Institute and State University, Virginia, USA, 2001.
- [19] P. Morin, C. Samson, J.-B. Pomet, and Z.-P. Jiang, "Time-varying feedback stabilization of the attitude of a rigid spacecraft with two controls," *Systems and Control Letters*, Vol. 25, 1995, pp. 375-385.
- [20] K. L. Musser and W. L. Ebert, "Autonomous spacecraft attitude control using magnetic torquing only," *Proceedings of Flight Mechanics/Estimation Theory Symposium*, 1989, pp. 23-38.
- [21] E.J Overby, *Attitude Control of Norwegian student satellite nCube*. Master's Thesis, Department of Engineering Cybernetics, Norwegian University of Science and Technology, Trondheim. 2004.
- [22] M. E. Pittelkau, "Optimal periodic control for spacecraft pointing and attitude determination," *AIAA Journal of Guidance, Control, and Dynamics*, Vol. 16, No. 6, 1993, pp. 1078-1084.

- [23] M. L. Psiaki, "Magnetic torquer attitude control via asymptotic periodic linear quadratic regulation," *AIAA Journal of Guidance, Control, and Dynamics*, Vol. 24, No. 2, 2001, pp. 386-394.
- [24] M. L. Renard, "Command laws for magnetic attitude control of spin-stabilized earth satellites," *Journal of Spacecraft and Rockets*, Vol. 4, No. 2, 1967, pp. 156-163.
- [25] M. Reyhanoglu, A. J. van der Schaft, N.H. McClamroch, and I. Kolmanovsky, "Dynamics and control of a class of underactuated mechanical systems," *IEEE Transactions on Automatic Control*, Vol. 44, No. 9, 1999, pp. 1663-1671.
- [26] M. Shigehara, "Geomagnetic attitude control of an axisymmetric spinning satellite," *Journal of Spacecraft and Rockets*, Vol. 9, No. 6, 1972, pp. 391-398.
- [27] J. A. Sorenson, "A Magnetic attitude control system for an axisymmetric spinning spacecraft," *Journal of Spacecraft and Rockets*, Vol. 8, No. 5, 1971, pp. 441-448.
- [28] P. Tsiotras, "Further passivity results for the attitude control problem," *IEEE Transactions on Automatic Control*, Vol. 43, No. 11, 1998, pp. 1597-1998.
- [29] P. Wang and Y. B. Shtessel, "Satellite attitude control using only magnetic torquers," *Proceedings of the AIAA Guidance, Navigation, and Control Conference*, 1998, pp. 1490-1498.
- [30] J. T.-Y. Wen and K. Kreutz-Delgado, "The attitude control problem," *IEEE Transactions on Automatic Control*, Vol. 36, No. 10, 1991, pp. 1148-1162.

- [31] J. Wertz, *Spacecraft attitude determination and control*, Kluwer Academic Publishers, 1978.
- [32] P. C. Wheeler, "Spinning spacecraft attitude control via the environmental magnetic field," *Journal of Spacecraft and Rockets*, Vol. 4, No. 12, 1967, pp. 1631-1637.
- [33] B. Wie, *Space Vehicle Dynamics and Control*, AIAA Education Series, 1998.
- [34] R. Wisniewski, *Satellite attitude control using only electromagnetic actuation*, Ph.D. Thesis, Aalborg University, Denmark, 1996.
- [35] R. Wisniewski and M. Blanke, "Fully magnetic attitude control for spacecraft subject to gravity gradient," *IFAC Journal Automatica*, Vol. 35, No. 7, 1999, pp. 1201-1214.

Appendix A

Simulink Diagram

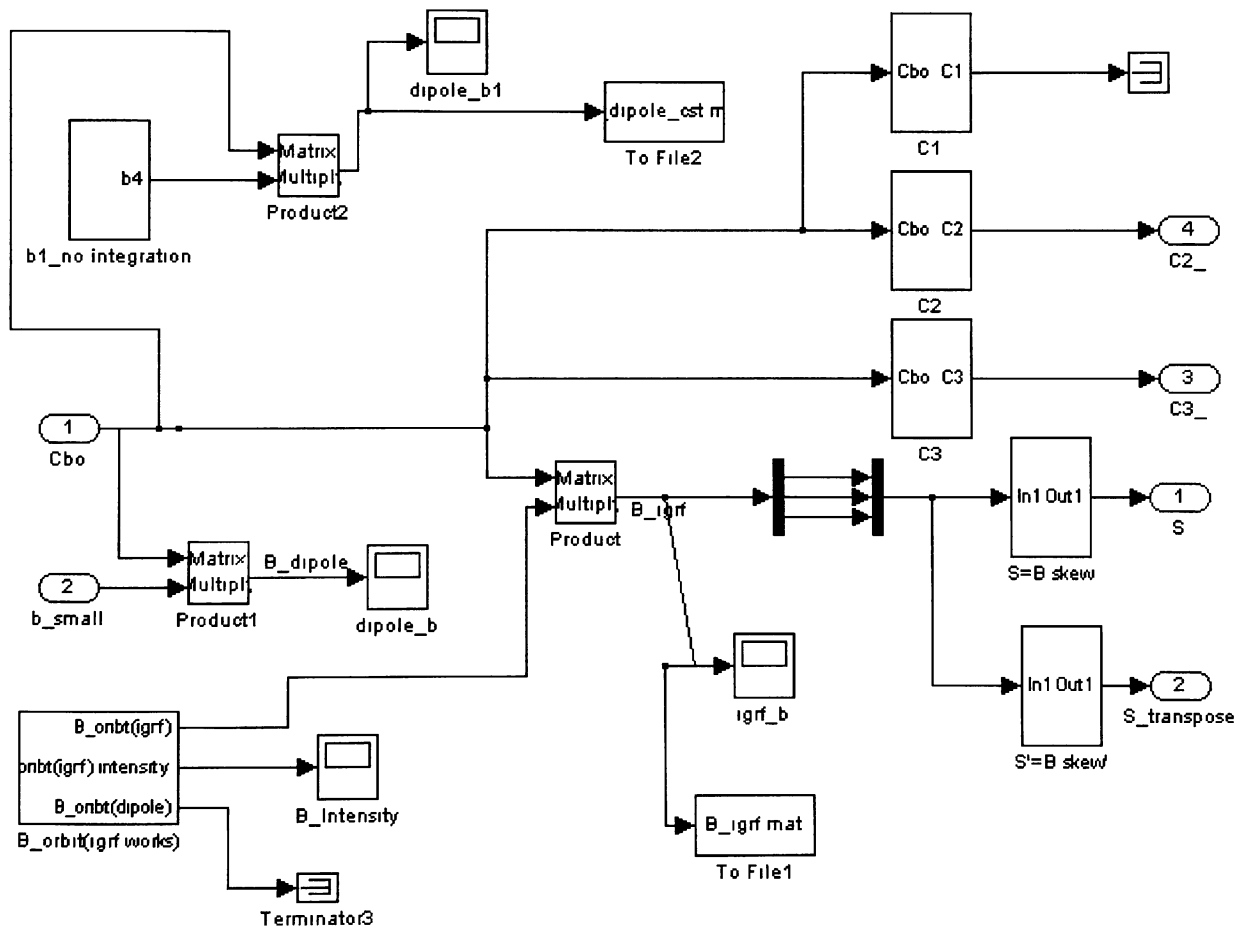


Figure A.1: Converting the magnetic field vector from Orbit frame to Body frame.

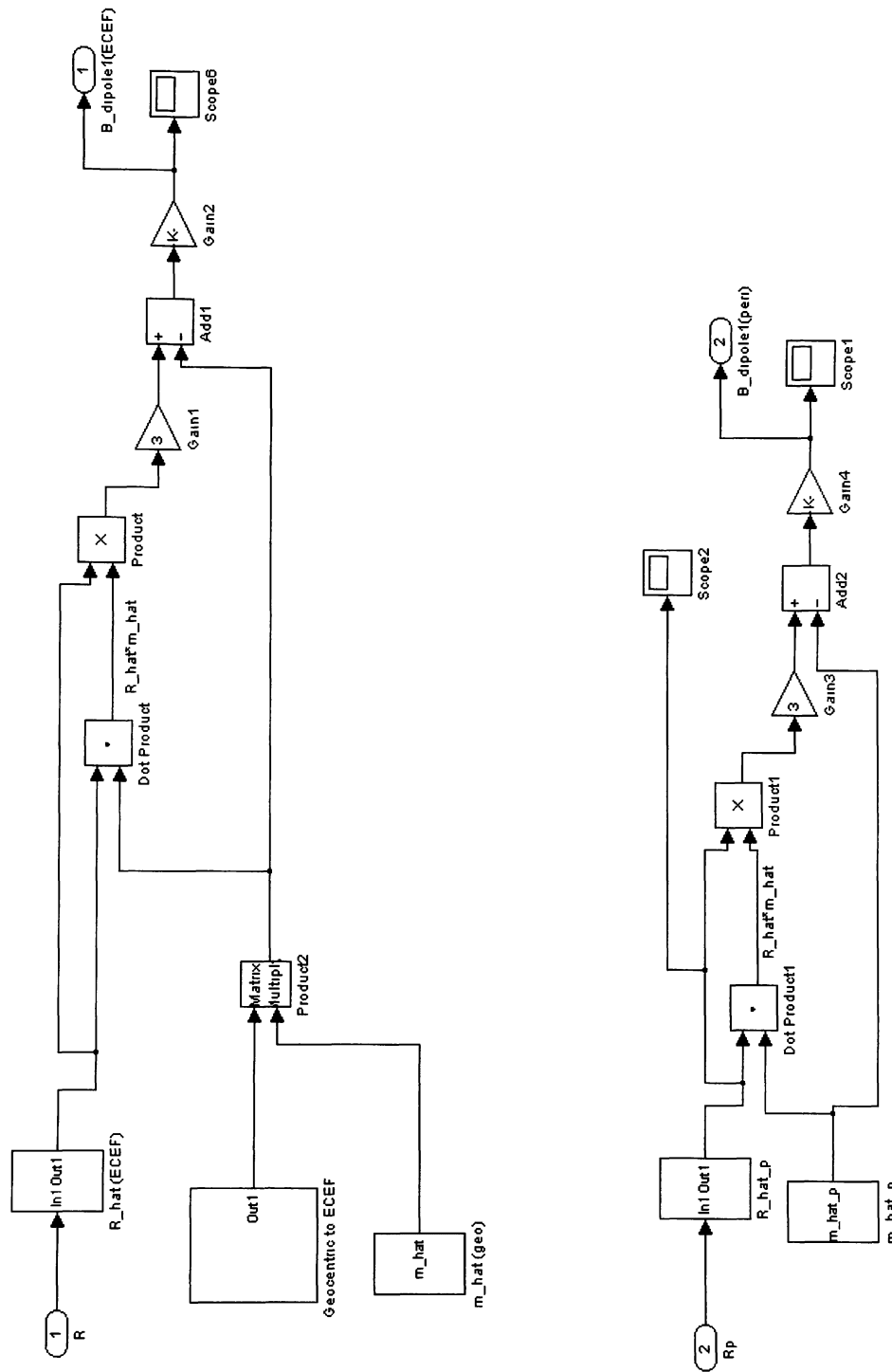


Figure A.2: Modeling the Tilted Dipole Magnetic Field from Perifocal frame and ECEF frame.

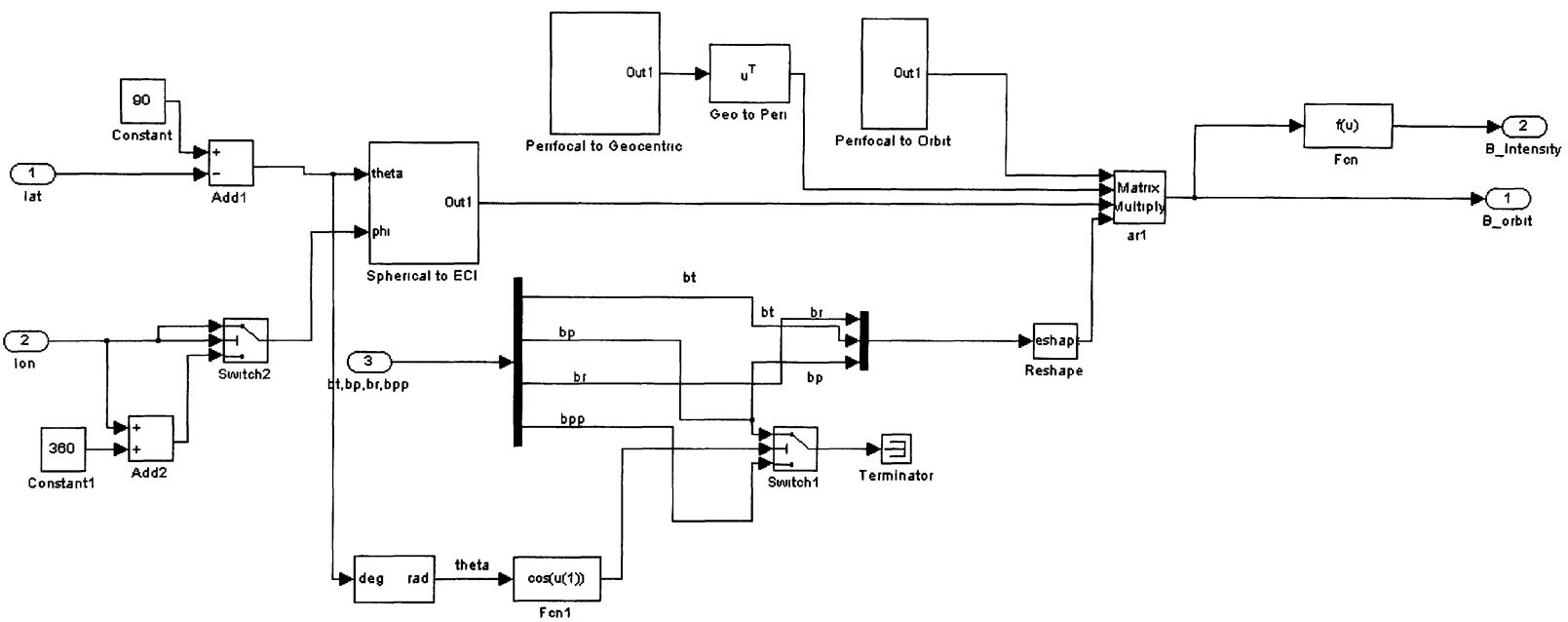


Figure A.3: Converting the IGRF model from ECI frame to Orbit frame.

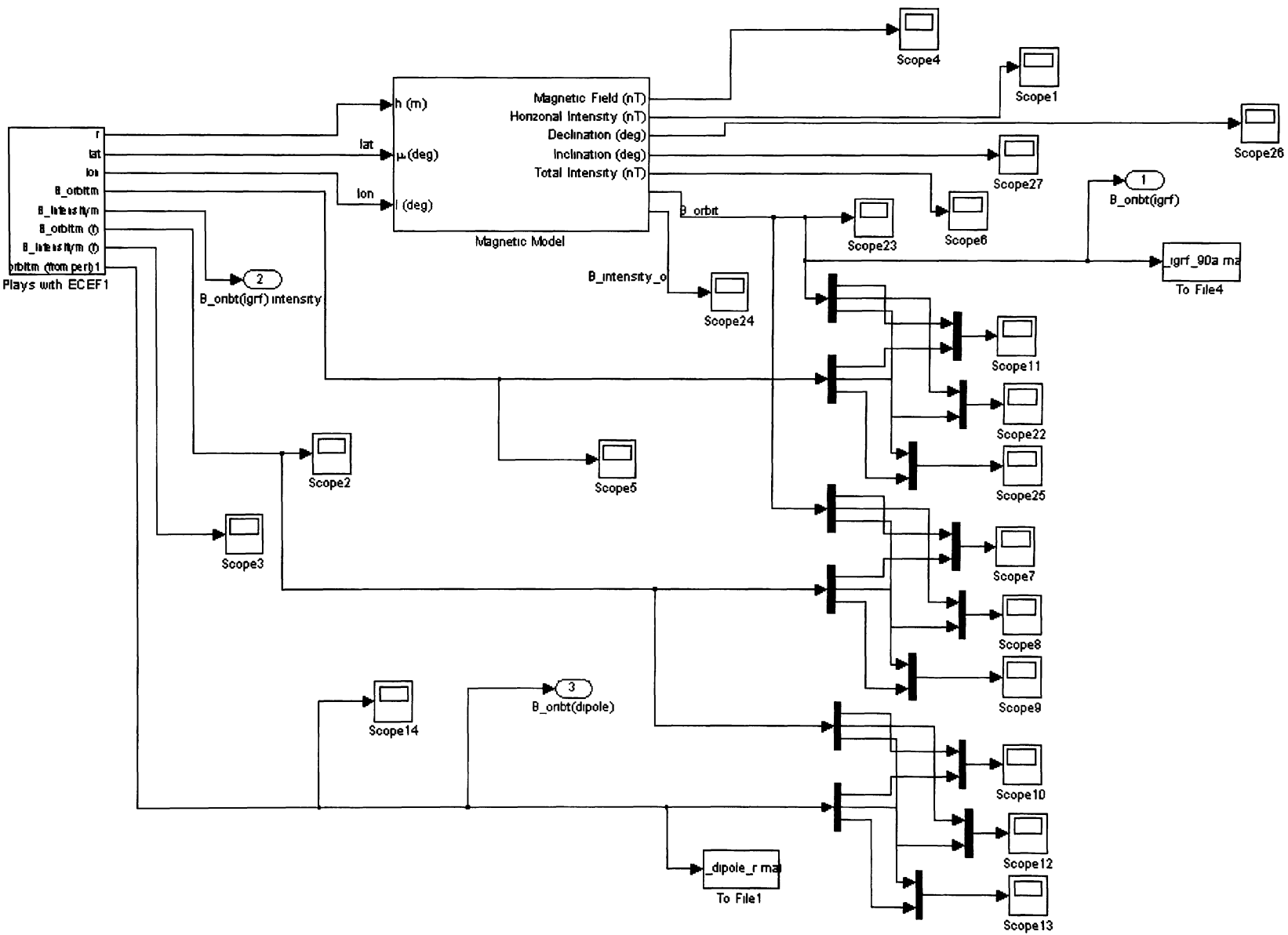


Figure A.4: Comparing the Tilted Dipole Model and the IGRF model in the Orbit frame.

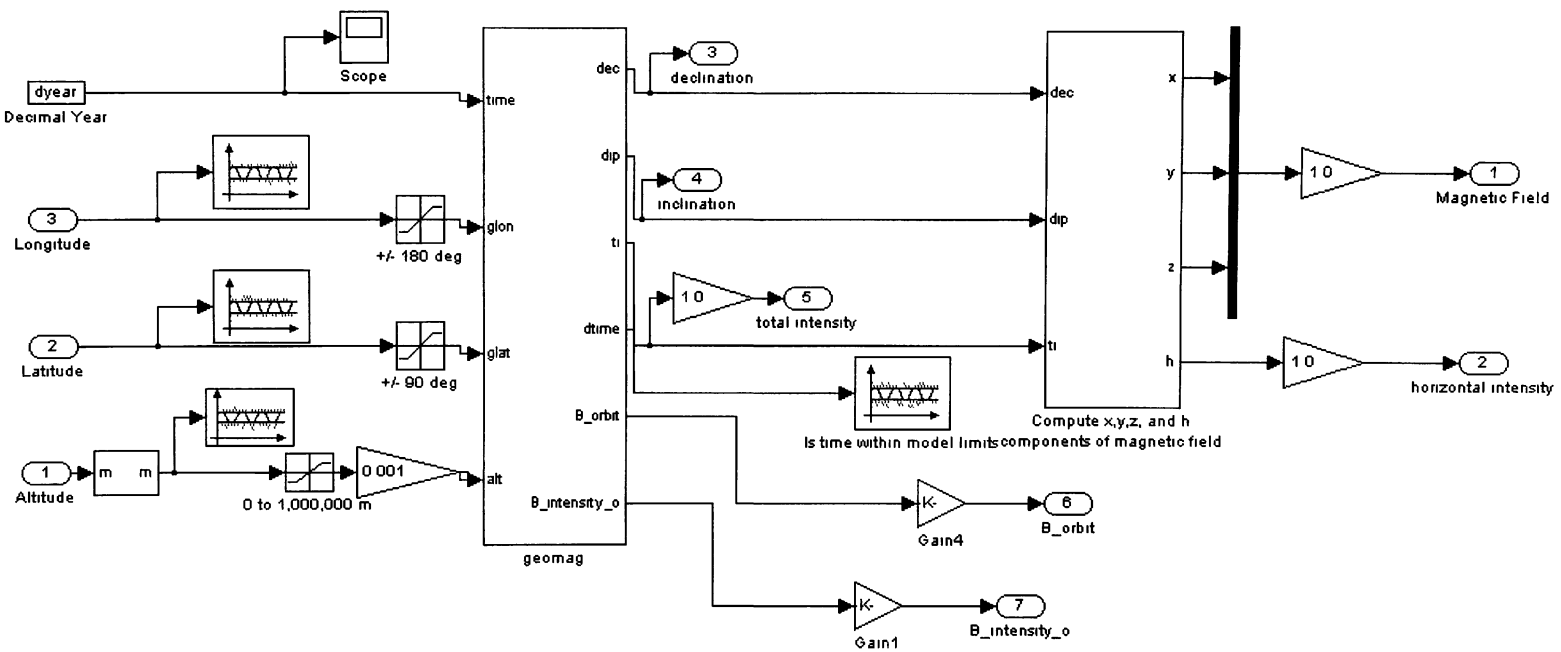


Figure A.5: Checking for longitude and latitude appropriate range and orbital radius Before going into magnetic field calculations.

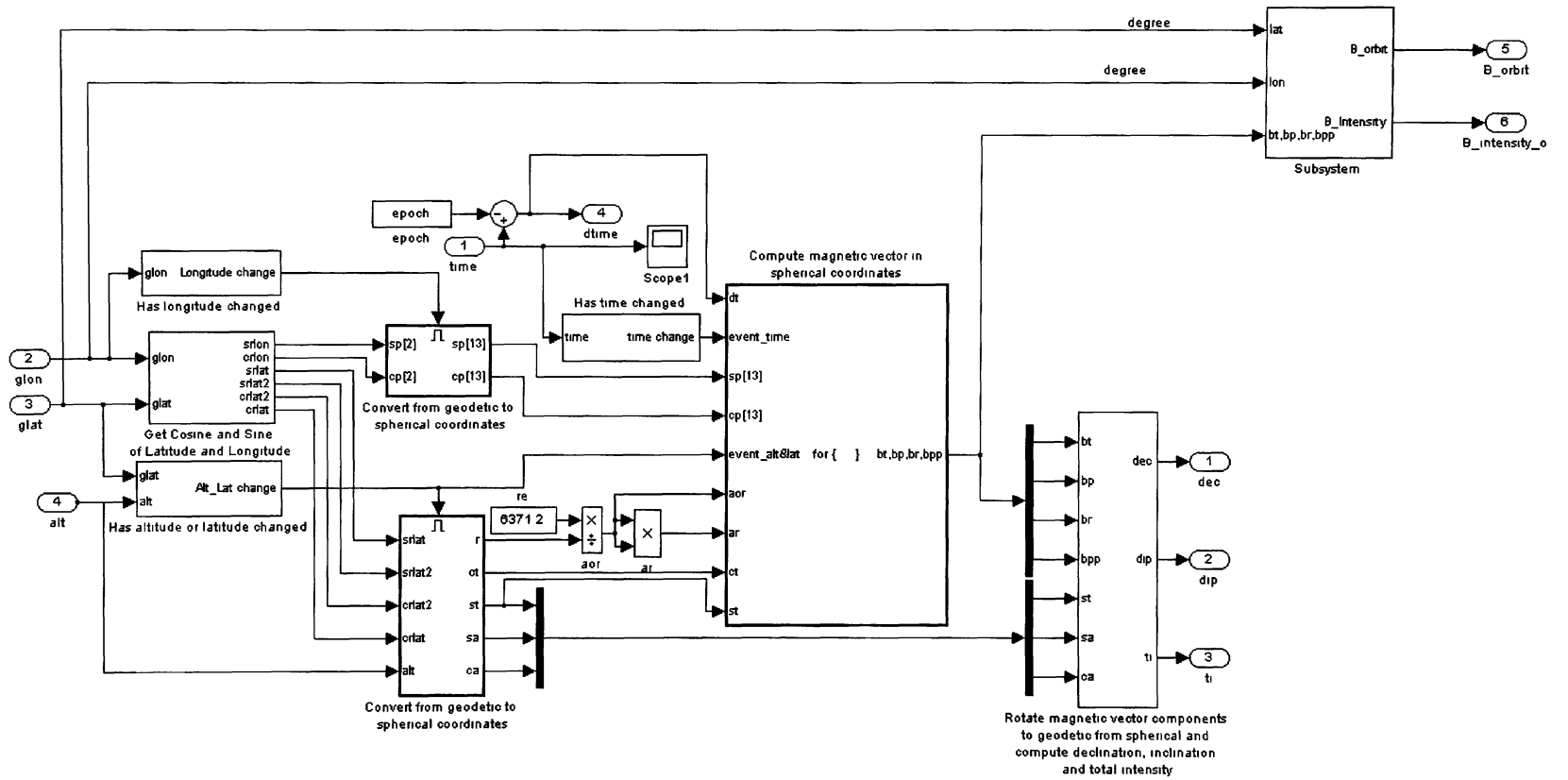


Figure A.6: Calculating the IGRF model.

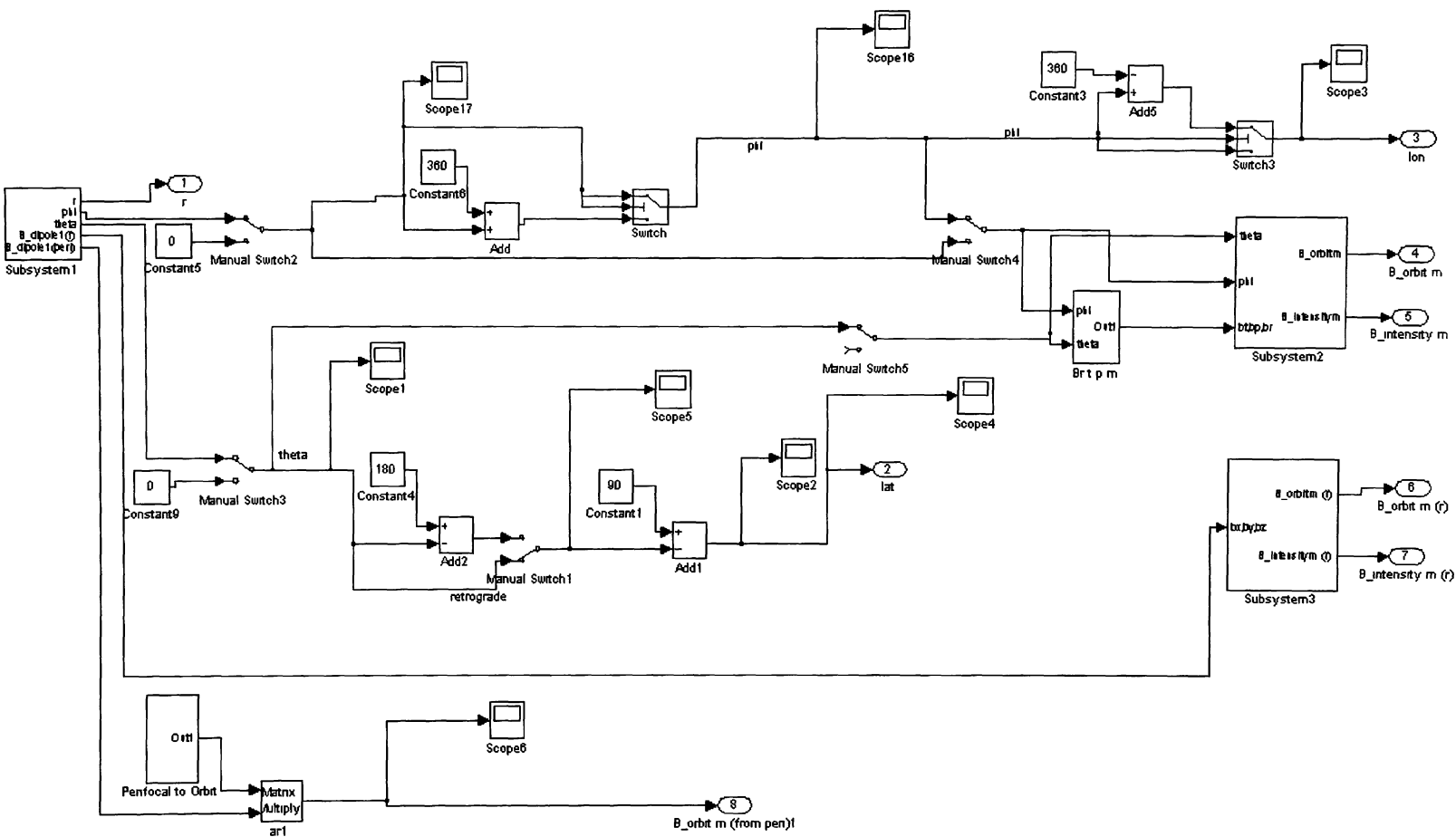


Figure A.7: Converting the Tilted Dipole Magnetic Field Model from Perifocal frame to Orbit frame.

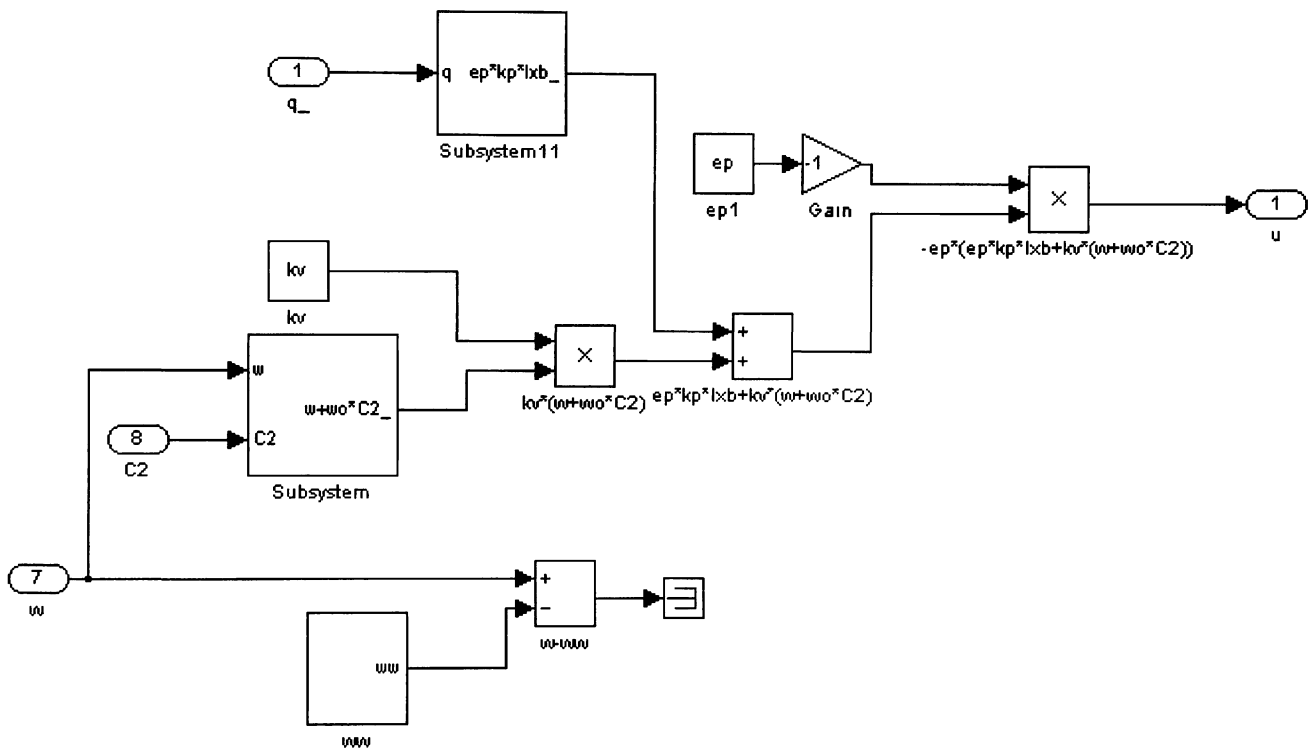


Figure A.8: Control Law for the Full-State Feedback.

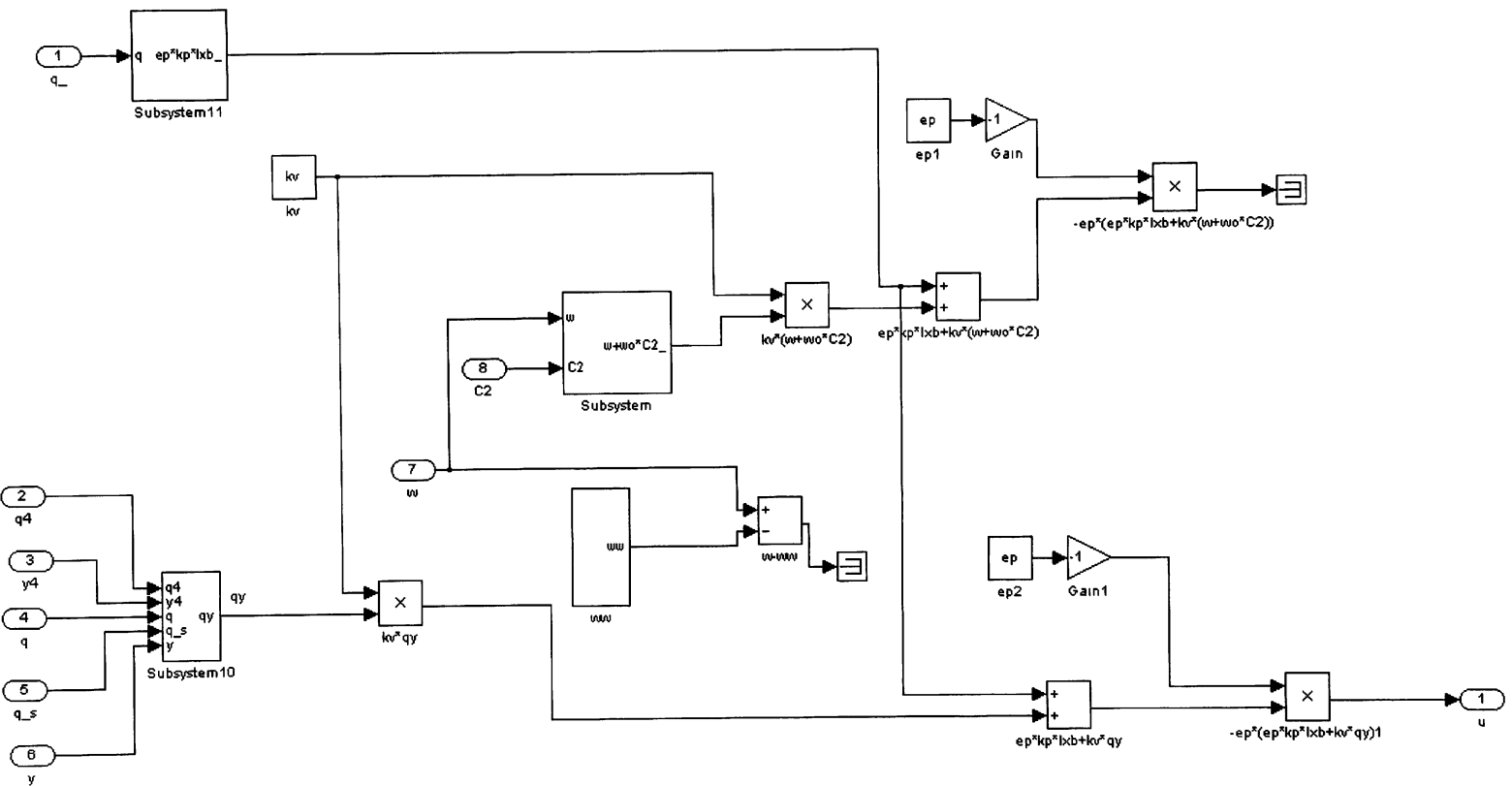


Figure A.9: Control Law for the Passivity-Based Feedback.

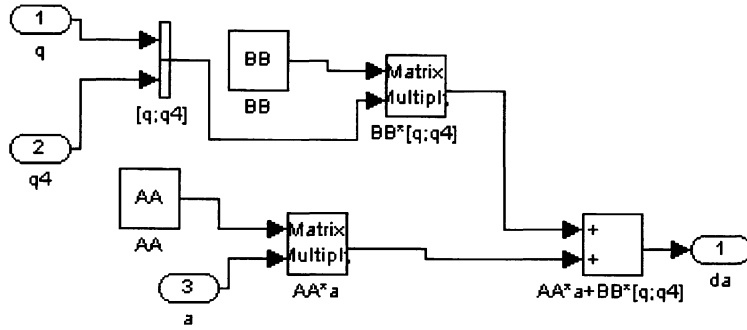


Figure A.10: The Control Filter State

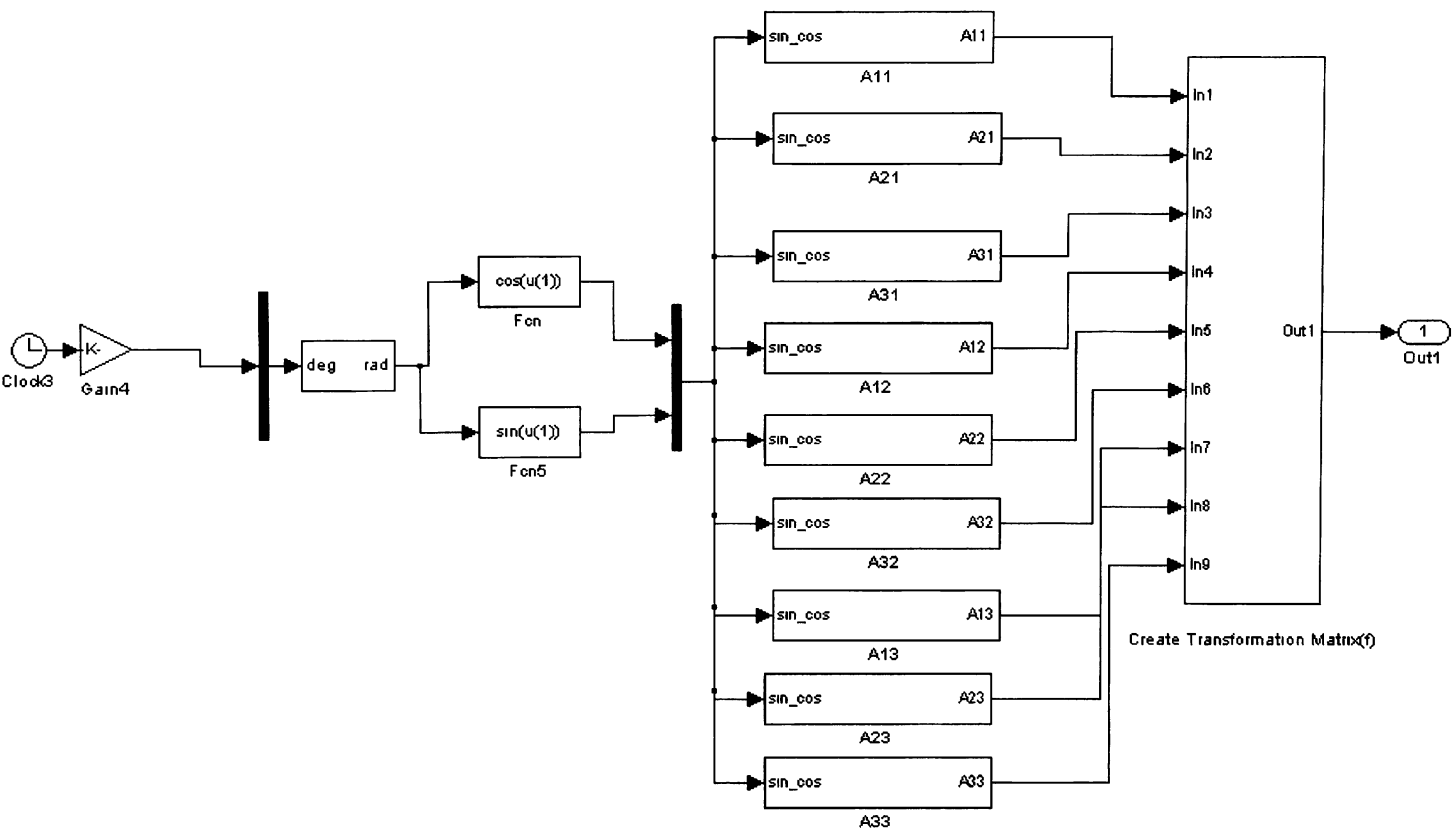


Figure A.11: Transformation Matrix from Geocentric frame to ECEF frame.

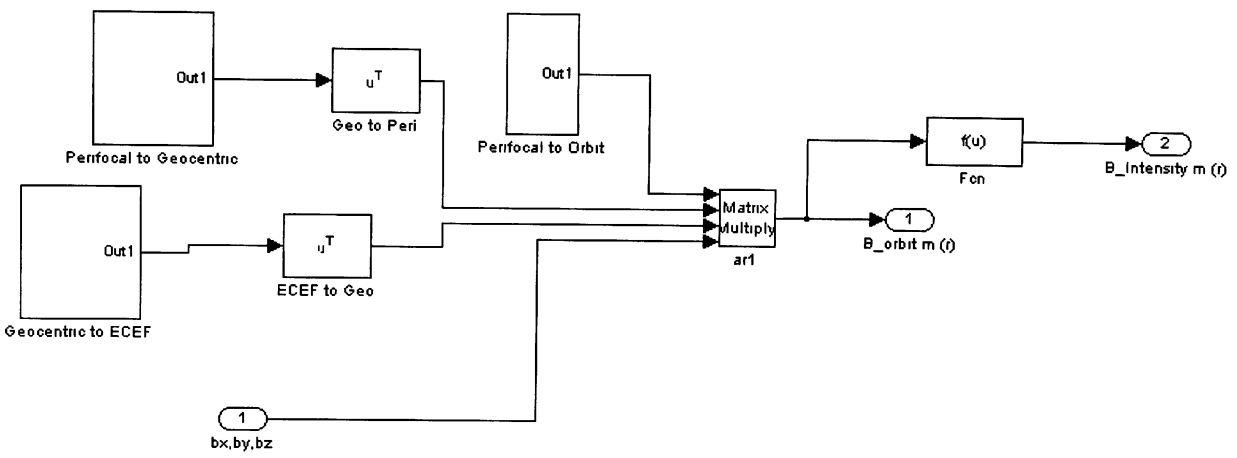


Figure A.12: Matrix Multiplication going from ECEF frame to Orbit frame.

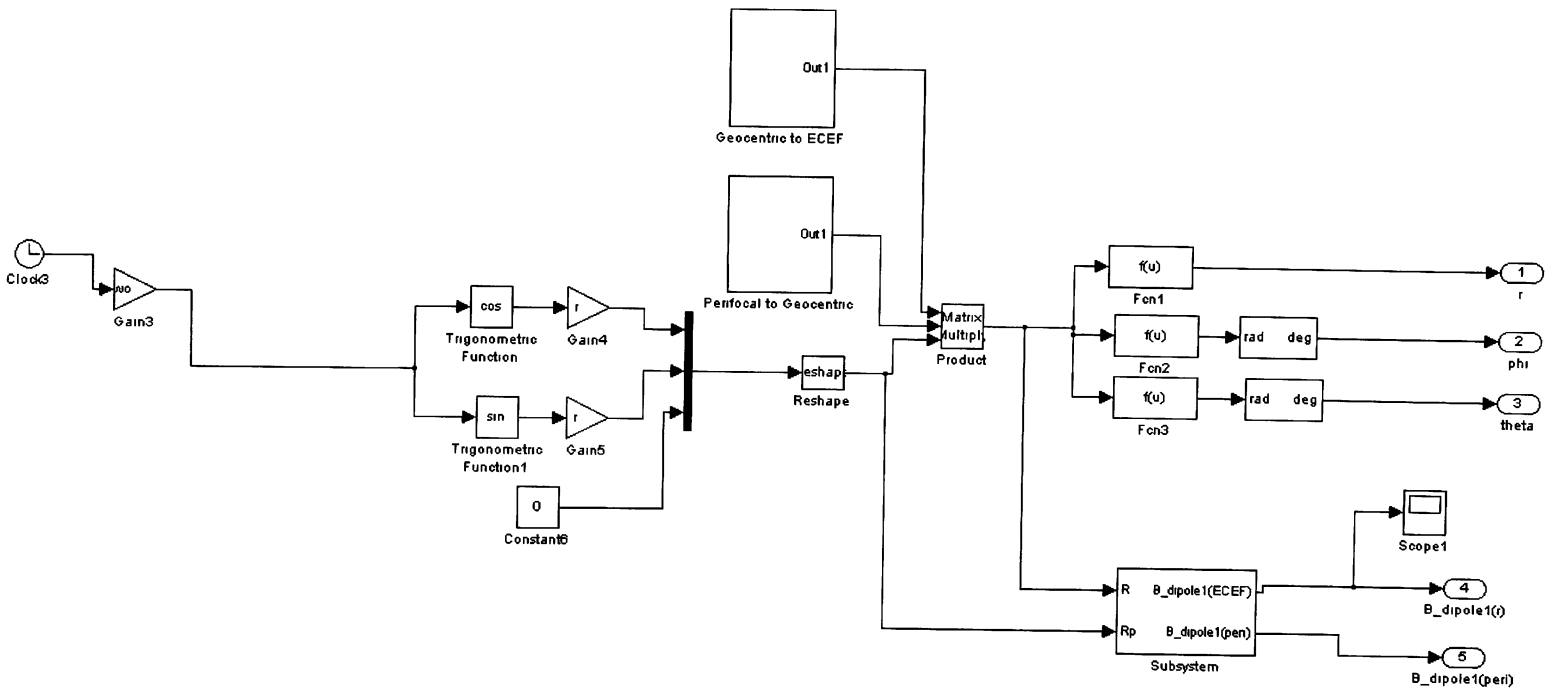
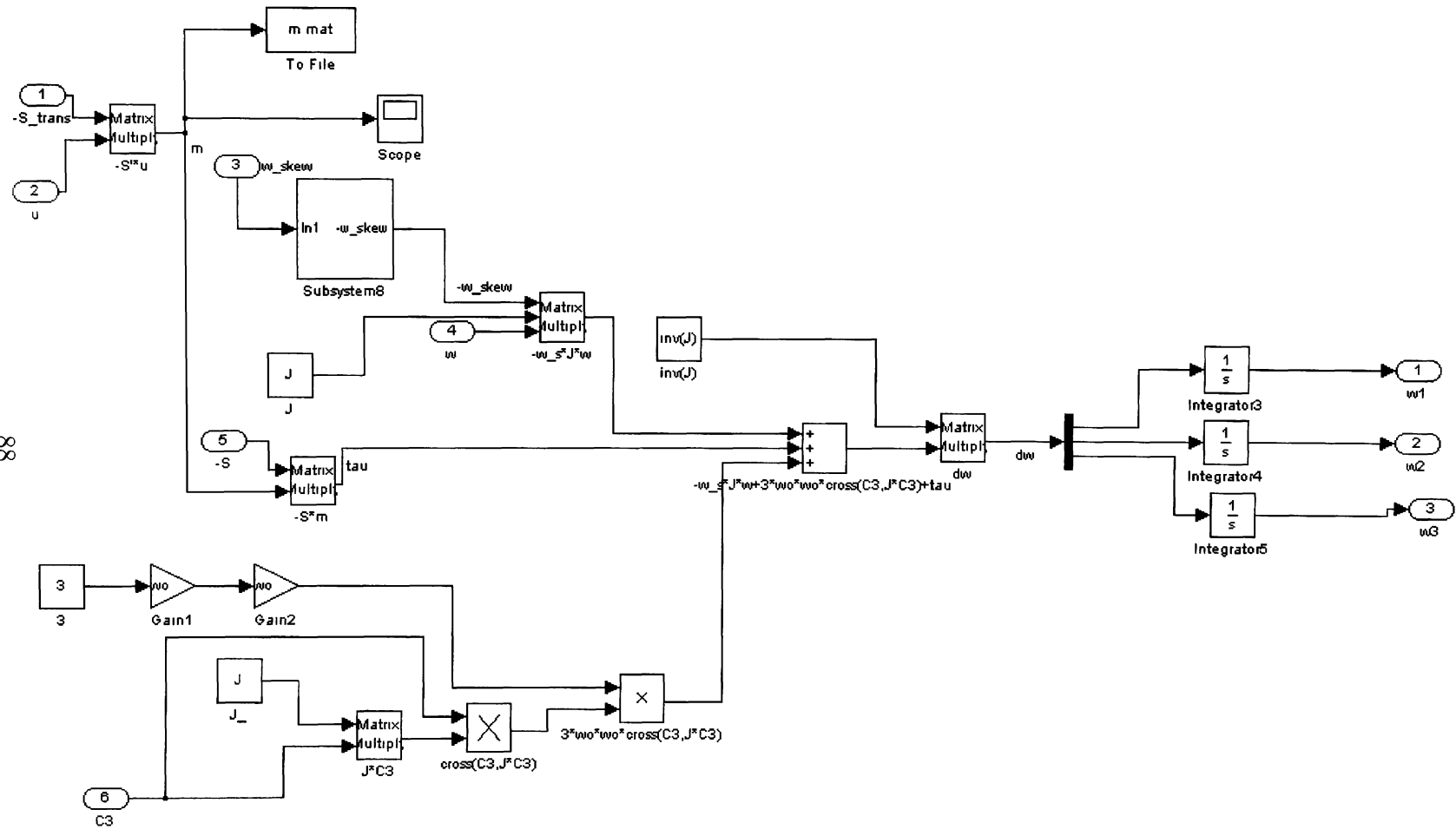


Figure A.13: The spacecraft's coordinate described in Perifocal frame

Figure A.14: Modeling of ω .



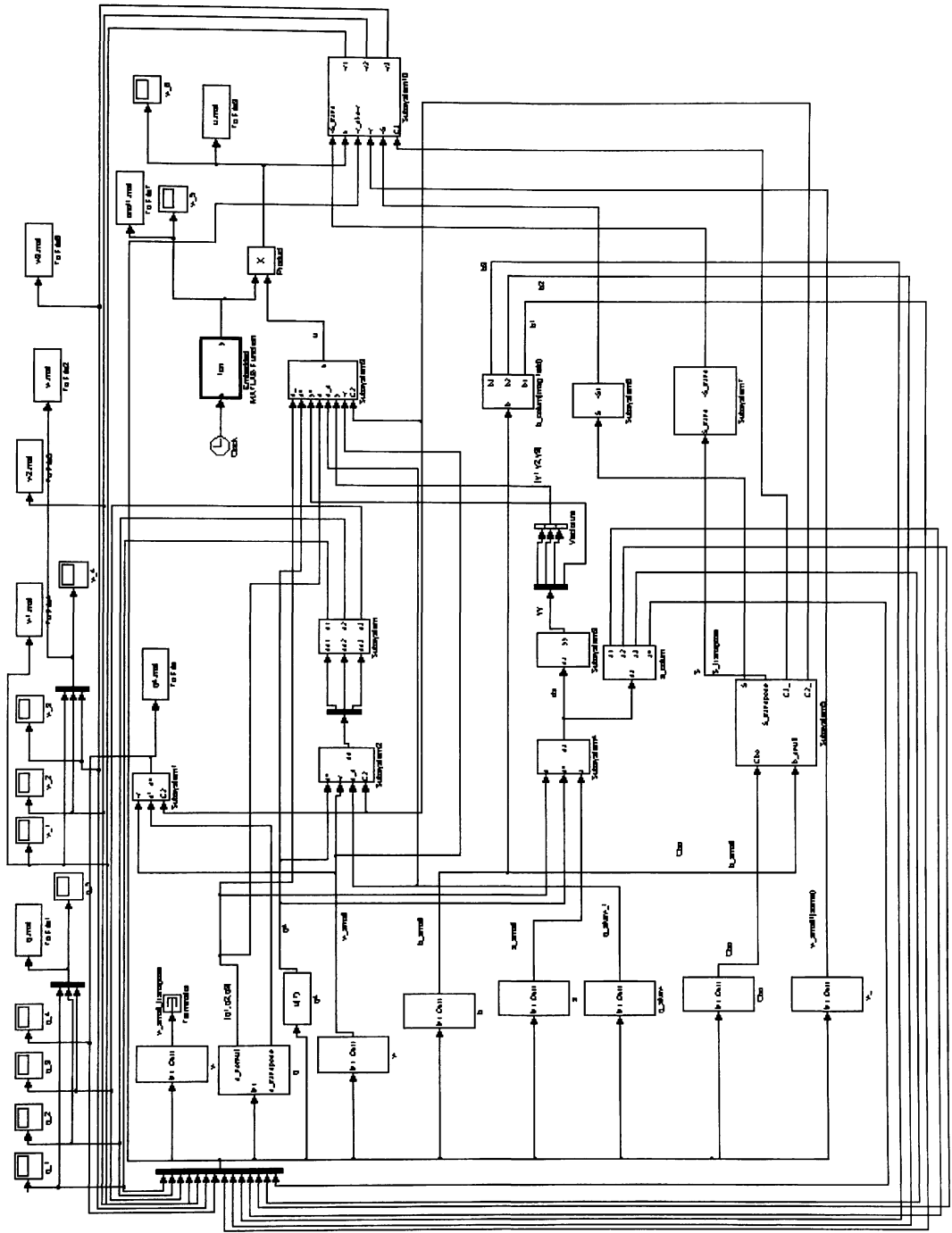


Figure A.15: Block diagram of the whole system.

Appendix B

Matlab m-file

This m-file contains the constants that's needed to be run before running the Simulink Model.

```
%Constants for simulink
clear; clc

A=eye(3);
J=[1/600 0 0;0 1/600 0;0 0 1/600];
J1=J(1); J2=J(2); J3=J(3);
AA=-1*eye(4);
BB=1*eye(4);
P=1*eye(4);
r=7000;
wo=0.00108;
ep=.0005;
kp=10^7;
kv=kp;

tmax=5828.5;

tspan=[0 tmax];

Bo=10^7/(r^3);
q0=[.5 .5 .5];
q40=sqrt(1-q0*q0');
w0=[.1 .1 .1];
b0=[Bo 0 0];
```

```

a0=[0 0 0 0];
k=1;

inc = 90 + 11.5;           %inclination angle (degrees)

r_ascen = 0;
perig = 0;
i_m = (inc-11.5)*pi/180;  %inclination angle with respect
                           %to the magnetic equator (rad)
w_e = 7.2921e-5;         %rad/sec
we=w_e;

re=6371.42;
g01 = -29556.8e-9;
g11 = -1671.8e-9;
h11 = 5080e-9;
Ho = sqrt(g01*g01 + g11*g11 + h11*h11);

%% For q_skew
Aq1 = [0 0 0; 0 0 -1; 0 1 0];
Aq2 = [0 0 1; 0 0 0; -1 0 0];
Aq3 = [0 -1 0; 1 0 0; 0 0 0];
%% For Transpose of skew for S
As1 = [0 0 0; 0 0 1; 0 -1 0];
As2 = [0 0 -1; 0 0 0; 1 0 0];
As3 = [0 1 0; -1 0 0; 0 0 0];

```